(CBF = 0.5 mL/g tissue/min, OEF = 0.4, CBV = 0.04, mL/g, p = 0.8 mL/g, Fv = 0.835, and R_{Hct} = 0.85) and an ischemic condition (CBF = 0.2 mL/g tissue/min, OEF = 0.7, CBV = 0.04 mL/g, p = 0.8 mL/g, Fv = 0.835, and R_{Hct} = 0.85). The tissue radioactivity from the residual $C^{15}O$ radioactivity was added to the simulated tissue TACs using Eq. 7. 100 sets of noisy tissue TACs were generated using an NEC model [19]. Figure 2 (right) shows a simulated tissue TAC under the condition of a time lag of 60 s and the case '100%'. For the subtraction method, $C_{True}(t)$ in Eq. 9 was computed for each dataset.

Calculation and evaluation of CBF and OEF values

The $H_2^{15}O$ contents (A_{H_2O}) and $^{15}O_2$ contents (A_{O_2}) were separated from the input functions using the separation method proposed by Kudomi et al. [16]. This separation is demonstrated in Fig. 3. The CBF and OEF values were computed from the A_{H_2O}, A_{O_2}, and the tissue TACs by means of Eqs. 4 and 5. The errors, in the form of bias and coefficient of variance (COV), in the estimated CBF and OEF values were calculated by comparing them with the true CBF and OEF values.

Results

Tables 1 and 2 show the results of the estimated values and COV for CBF and OEF in this simulation study using the conventional DARG method in the cases of the normal model and ischemic model, respectively. As shown in these tables, the estimated CBF and OEF values were underestimated in all cases due to the residual $C^{15}O$ radioactivity. For instance, in the case of the normal model and a time lag of 60 s, the underestimation of the estimated OEF value

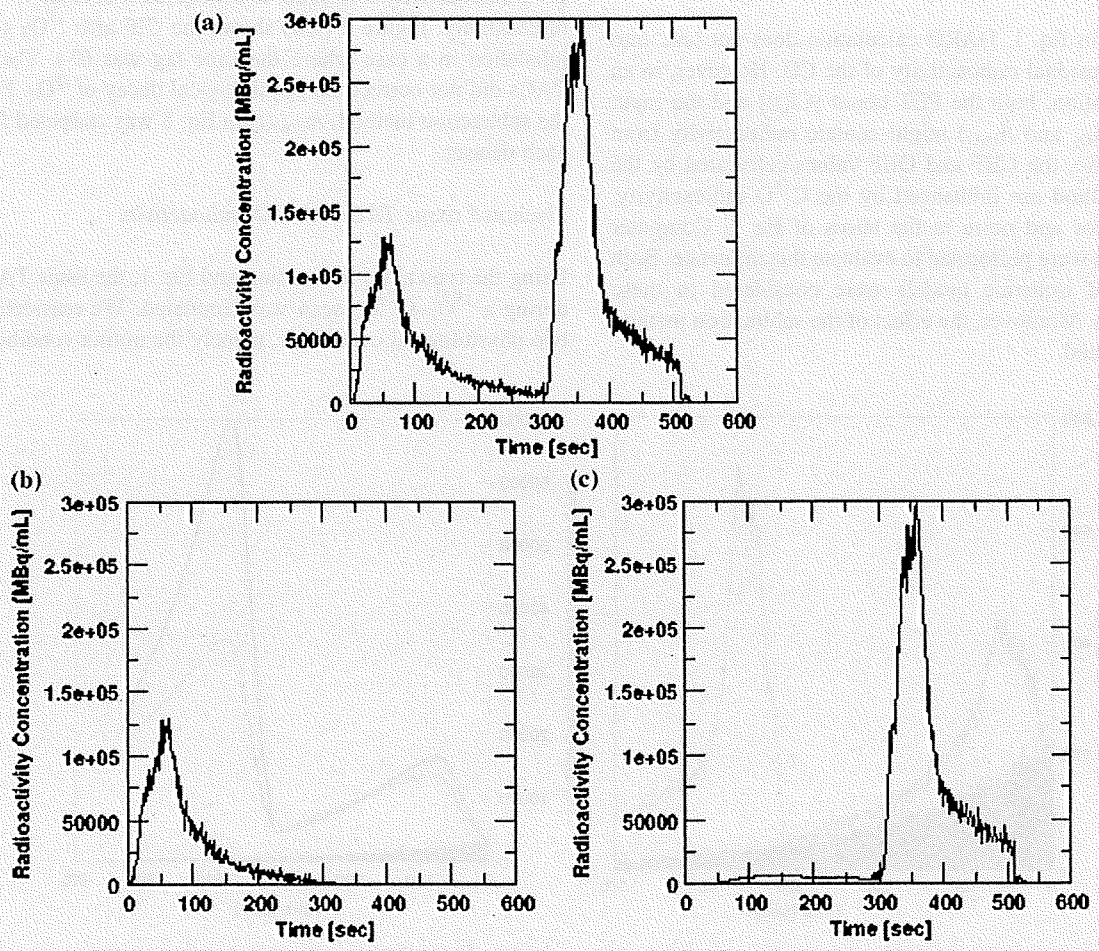

Fig. 3 Separation of the input function for the $^{15}O_2$–$C^{15}O_2$ scan. Total input function (**a**), $^{15}O_2$ input function (**b**), and $C^{15}O_2$ input function (**c**) separated from the total input function. The radioactivity observed earlier than 300 s in the graph (**c**) is the recirculation water

Table 1 Summary of simulation for CBF and OEF in the case '25%' and the case '100%' of the normal model using the conventional DARG method

$C^{15}O$–$^{15}O_2$ time lag (s)	CBF			OEF		
	Average (mL/g/min)	Error (%)	COV (%)	Average	Error (%)	COV (%)
Case '25%'						
60	0.49	−2.06	1.07	0.30	−25.0	1.06
100	0.49	−1.82	0.66	0.31	−21.0	0.52
200	0.50	−0.12	0.23	0.35	−13.5	0.33
400	0.50	−0.04	0.17	0.38	−4.55	0.19
800	0.50	−0.02	0.06	0.40	−0.48	0.07
Case '100%'						
60	0.46	−7.55	1.68	0.16	−60.9	1.64
100	0.47	−6.05	1.37	0.18	−54.4	1.25
200	0.48	−3.91	0.92	0.25	−38.7	0.823
400	0.49	−1.51	0.42	0.34	−16.0	0.45
800	0.50	−0.19	0.08	0.39	−1.90	0.12

Table 2 Summary of simulation for CBF and OEF in the case '25%' and the case '100%' of ischemic model using the conventional DARG method

$C^{15}O$–$^{15}O_2$ time lag (s)	CBF			OEF		
	Average (mL/g/min)	Error (%)	COV (%)	Average	Error (%)	COV (%)
Case '25%'						
60	0.20	−2.72	0.30	0.55	−21.3	0.48
100	0.20	−2.18	0.26	0.58	−17.8	0.37
200	0.20	−1.30	0.17	0.62	−10.9	0.30
400	0.20	−0.45	0.07	0.67	−3.83	0.16
800	0.20	−0.04	0.02	0.70	−0.39	0.06
Case '100%'						
60	0.18	−8.27	0.88	0.33	−52.6	1.08
100	0.19	−6.84	0.71	0.37	−46.9	0.85
200	0.19	−4.43	0.43	0.47	−33.1	0.62
400	0.20	−1.70	0.18	0.61	−13.6	0.36
800	0.20	−0.20	0.04	0.69	−1.60	0.11

was −25% for the case '25%' and −61% for the case '100%'. Larger underestimation values were observed for shorter time lags. The OEF estimation was more sensitive to the residual CO radioactivity than the CBF estimation. Less underestimation was observed in the CBF value in the normal model than in the ischemic model. On the other hand, a larger underestimation was observed in the OEF value in the normal model compared to the ischemic model. The COV was always larger in the normal model than in the ischemic model.

Tables 3 and 4 show the results of the estimated values and the COV for CBF and OEF using the subtraction method. As shown in the tables, no underestimation was observed in all cases. Moreover, the COV values were less than one by the conventional method.

Discussion

CBV images are widely used for the diagnosis of cerebrovascular disease [20]. These images are also utilized to correct the vascular space in the DARG method for CBF and OEF values [15]. Therefore, a $C^{15}O$ scan is mandatory for the DARG protocol. Due to a desire to shorten the total study period, it is often observed that the $^{15}O_2$–$C^{15}O_2$ scan is initiated without waiting long enough for the physical decay of the $C^{15}O$ radioactivity. In this paper, the influences of this residual $C^{15}O$ radioactivity on the CBF and OEF values for the DARG protocol were evaluated by means of computer simulations. According to the results, the CBF and OEF values were underestimated because of the residual $C^{15}O$ radioactivity. The magnitude of the

Table 3 Summary of simulation for CBF and OEF in the case '25%' and the case '100%' of normal model using the DARG method with the subtraction method

$CO–O_2$ time lag (s)	CBF			OEF		
	Average (mL/g/min)	Error (%)	COV (%)	Average	Error (%)	COV (%)
Case '25%'						
60	0.50	0.15	0.37	0.40	−0.17	0.54
100	0.50	0.16	0.33	0.40	−0.18	0.41
200	0.50	0.08	0.27	0.40	−0.31	0.34
400	0.50	−0.04	0.13	0.40	−0.60	0.18
800	0.50	0.02	0.04	0.40	0.12	0.07
Case '100%'						
60	0.50	0.28	0.53	0.40	−0.24	1.02
100	0.50	0.32	0.53	0.40	−0.45	0.97
200	0.50	0.17	0.40	0.40	−0.61	0.70
400	0.50	0.04	0.27	0.40	−0.34	0.41
800	0.50	−0.02	0.07	0.40	−0.17	0.12

Table 4 Summary of simulation for CBF and OEF in the case '25%' and the case '100%' of ischemic model using the DARG method with the subtraction method

$CO–O_2$ time lag (s)	CBF			OEF		
	Average (mL/g/min)	Error (%)	COV (%)	Average	Error (%)	COV (%)
Case '25%'						
60	0.20	0.05	0.15	0.70	−0.13	0.46
100	0.20	0.05	0.14	0.70	−0.14	0.36
200	0.20	0.00	0.11	0.70	−0.25	0.29
400	0.20	−0.05	0.06	0.70	−0.51	0.16
800	0.20	0.01	0.02	0.70	0.11	0.06
Case '100%'						
60	0.20	0.09	0.25	0.70	−0.22	0.86
100	0.20	0.10	0.24	0.70	−0.36	0.83
200	0.20	0.03	0.17	0.70	−0.50	0.62
400	0.20	−0.01	0.11	0.70	−0.27	0.36
800	0.20	−0.02	0.04	0.70	−0.15	0.11

underestimation depended on the amount of $C^{15}O$ radioactivity, the time interval between the $C^{15}O$ scan and the $^{15}O_2$–$C^{15}O_2$ scan, and the disease model we assumed. By subtracting the $C^{15}O$ radioactivity from the input function and PET counts, this underestimation could be eliminated, which resulted in shortening the total study period of the DARG protocol.

Underestimation of CBF and OEF values due to residual $C^{15}O$ radioactivity

In general, overestimations of the arterial radioactivity or PET counts can cause underestimation or overestimation of physiological measures (CBF and OEF), respectively, in the DARG method. Thus, the residual $C^{15}O$ radioactivity might induce the bias in either of direction. As shown in our results, the estimated CBF and OEF values were both underestimated due to the residual $C^{15}O$ radioactivity, which indicates that the bias of the input function by the $C^{15}O$ radioactivity more strongly influenced the estimates than the bias of the PET counts by the $C^{15}O$ radioactivity. In our simulation, the CBV was fixed as 0.04 mL/mL. If the larger CBV was assumed (i.e. dilatation of blood vessel), more residual $C^{15}O$ radioactivity was added on the PET counts and the bias of the total PET counts was increased by Eq. 1, which results in less underestimation for the CBF and OEF values. Note that in this paper, we evaluated not $CMRO_2$ but OEF. $CMRO_2$ is derived by being multiplied CBF and OEF values. Thus, the magnitude of the underestimation in $CMRO_2$ could be larger than those of CBF and OEF.

Tables 1 and 2 suggest that the normal model underestimated OEF more than the ischemic model because of the residual $C^{15}O$ radioactivity. On other hand, the normal

model underestimated CBF less than the ischemic model because of the residual $C^{15}O$ radioactivity. Although the DARG method uses $^{15}O_2$ phase (PET data before the inhalation of $C^{15}O_2$) and $C^{15}O_2$ phase (PET data after the inhalation of $C^{15}O_2$) datasets, and simultaneously estimates CBF and OEF values, the PET data of the $^{15}O_2$ phase were dominant in the determination of OEF and those of the $C^{15}O_2$ phase were dominant in the determination of CBF. As shown in Tables 1 and 2, the amount of the underestimation for OEF is larger than for CBF, which can be explained by the amount of residual $C^{15}O$ radioactivity in both phases. As shown in Fig. 2, the influence of $C^{15}O$ on the input function was much higher in the $^{15}O_2$ phase than in the $C^{15}O_2$ phase. The residual $C^{15}O$ radioactivity led to the underestimation of CBF, mainly determined in the $C^{15}O_2$ phase. However, this underestimation was not enough to explain the bias of the input function in the $^{15}O_2$ phase. The first term on the right side of Eq. 1 has only CBF (f) as a parameter and the value of the first term is much higher in the normal model than in the ischemic model due to the higher CBF of the normal model, which implies that a greater underestimation for OEF could occur in the normal model to compensate for the insufficient underestimation of CBF. The ischemic model has a lower CBF than the normal model, which results in the slow washout of $^{15}O_2$ in tissue (the second term on the right side of Eq. 1). Therefore, the ischemic model has a greater source of underestimation for CBF than the normal model during the $C^{15}O_2$ phase.

As shown in Tables 1, 2, 3, and 4, the COVs of CBF and OEF in the ischemic model were smaller than the COVs in the normal model. The non-linear relationship between the PET counts and CBF attributed to this phenomenon [13]. The PET counts of the normal model were higher than those of the ischemic model, and the higher PET counts emphasized the noise due to this non-linearity.

Our results suggest that attention must be paid to the interpretation of CBF and OEF images from DARG, if contaminated by the significant amount of the residual $C^{15}O$ radioactivity namely: the magnitude of the error may not be uniform across different physiological conditions in the brain.

Subtraction method

The subtraction method successfully eliminated the influence of the $C^{15}O$ radioactivity on both the input function and PET counts during the $^{15}O_2$–$C^{15}O_2$ scan, and no errors in the CBF and OEF values due to the residual $C^{15}O$ radioactivity were observed. In theory, there is no statistical advantage for the subtraction method compared to the conventional method. However, as shown in Tables 3 and 4, the COV by the subtraction method was smaller than the value by the conventional method. It is necessary to separate the $^{15}O_2$ contents and $C^{15}O_2$ contents in the measured input function prior to the DARG calculation. For this separation, we utilized the linear method proposed by Kudomi et al. [16]. The linear method estimates the $^{15}O_2$ contents in the input function after $C^{15}O_2$ inhalation by linear extrapolation. In the conventional method, due to the offset of the input function by the residual $C^{15}O$ radioactivity, the estimated $^{15}O_2$ contents remain until the last in most cases. On other hand, in the subtraction method, by subtracting the $C^{15}O$ radioactivity from the input function, the offset of the input function is removed. Then, in many cases the $^{15}O_2$ contents estimated by the extrapolated line go to zero. This causes a reduction of the variation in the estimated CBF and OEF values compared to the conventional method.

The estimation of the recirculation water in the input function is based on the empirical model [10], and this model may not work owing to the residual $C^{15}O$ radioactivity, which results in biased CBF and OEF values. This bias can be removed by the subtraction method. Thus, by using the subtraction method, accurate CBF and OEF values can be measured no matter how much $C^{15}O$ radioactivity exists, which results in shortening the total PET study. The subtraction method could be applied, not only to the DARG protocol, but also to the conventional ARG and steady-state protocols. In this simulation, we assumed no biological decay of $C^{15}O$, which is not true in the actual data, and the subtraction method might over-subtract the influence of $C^{15}O$ radioactivity. The biological half-life of $C^{15}O$ is difficult to determine within a period of ordinary PET scan owing to the short life of the ^{15}O radionuclide. We tested simulated data with a biological half-life of 10 min, and there were no significant differences in the estimated CBF and OEF values compared to the results shown in this paper. In order to apply the subtraction method in clinical study, further studies are, however, required to verify the influence of biological decay.

Sequence of PET scans

In this paper, the sequence of the scans was a $C^{15}O$ scan followed by a $^{15}O_2$–$C^{15}O_2$ scan. If the $C^{15}O$ scan was performed after the $^{15}O_2$–$C^{15}O_2$ scan, our results were not valid. The reason for this sequence ($C^{15}O$ scan followed by a $^{15}O_2$–$C^{15}O_2$ scan) was to shorten the total duration of the PET study by exchanging the target gas (from N_2 containing O_2 to N_2 containing CO_2) only once (the synthesis of $C^{15}O$ and $^{15}O_2$ shares the same target in a cyclotron but uses different one from that of $C^{15}O_2$). Furthermore, the sequence of $^{15}O_2$–$C^{15}O_2$ produces better results than the sequence of $C^{15}O_2$–$^{15}O_2$ [15]. In order to further shorten the total study time, more development efforts are needed

in relation to the delivery system for the radioactive gases, which should have the ability to deliver such gases quickly.

The results in this paper were based only on the computer simulations. It could be expected to have several difficulties to show validities of our results using actual PET measurements by several reasons such as (1) PET cannot differentiate between photon from residual $C^{15}O$ and photon from either $^{15}O_2$ or $C^{15}O_2$, (2) large inter-subject variation for cerebrovascular disease, (3) large amounts of radiation exposure to patients from $C^{15}O$ in the case of large inhalation of $C^{15}O$. For the validation of our results, PET studies with ischemic animal model will be anticipated.

Conclusions

In this paper, we verified the influence of $C^{15}O$ radioactivity on the computation of CBF and OEF using the DARG protocol. We found that the bias and noise in the CBF and OEF values depended on the amount of residual $C^{15}O$ radioactivity during the scanning for $^{15}O_2$ and $C^{15}O_2$, and on the physiological conditions of the brain tissue. By using the subtraction method, the bias could be eliminated. Finally, we discussed the effects of the recirculation water and the biological decay for $C^{15}O$ radioactivity on the computation of CBF and OEF using the DARG method.

References

1. Frackowiak RS, Jones T, Lenzi GL, Heather JD. Regional cerebral oxygen utilization and blood flow in normal man using oxygen-15 and positron emission tomography. Acta Neurol Scand. 1980;62:336–44.
2. Frackowiak RS, Lenzi GL, Jones T, Heather JD. Quantitative measurement of regional cerebral blood flow and oxygen metabolism in man using 15O and positron emission tomography: theory, procedure, and normal values. J Comput Assist Tomogr. 1980;4:727–36.
3. Mintun MA, Raichle ME, Martin WR, Herscovitch P. Brain oxygen utilization measured with O-15 radiotracers and positron emission tomography. J Nucl Med. 1984;25(2):177–87.
4. Lammertsma AA, Jones T. Correction for the presence of intravascular oxygen-15 in the steady-state technique for measuring regional oxygen extraction ratio in the brain: 1. Description of the method. J Cereb Blood Flow Metab. 1983;3:416–24.
5. Subramanyam R, Alpert NM, Hoop B Jr, Brownell GL, Yaveras JM. A model for regional cerebral oxygen distribution during continuous inhalation of 15O2, C15O, and C15O2. J Nucl Med. 1978;19:48–53.
6. Lammertsma AA, Heather JD, Jones T, Frackowiak RS, Lenzi GL. A statistical study of the steady state technique for measuring regional cerebral blood flow and oxygen utilization using 15O. J Comput Assist Tomog. 1982;6:566–73.
7. Correia JA, Alpert NM, Buxton RB, Ackerman RH. Analysis of some errors in the measurement of oxygen extraction and oxygen consumption by the equilibrium inhalation method. J Cereb Blood Metab. 1985;5:591–9.
8. Okazawa H, Ymauchi H, Sugimoto K, Takahashi M, Toyoda H, Kishibe Y, et al. Quantitative comparison of the bolus and steady-state methods for measurement of cerebral perfusion and oxygen metabolism: positron emission tomography study using 15O-gas and water. J Cereb Blood Metab. 2001;21:793–803.
9. Okazawa H, Ymauchi H, Sugimoto K, Toyoda H, Kishibe Y, Takahashi M. Effects of acetazolamide on cerebral blood flow, blood volume, and oxygen metabolism: a positron emission tomography study with healthy volunteers. J Cereb Blood Flow Metab. 2001;21:1472–9.
10. Iida H, Jones T, Miura S. Modeling approach to eliminate the need to separate arterial plasma in oxygen-15 inhalation positron emission tomography. J Nucl Med. 1993;34:1333–40.
11. Sadato N, Yonekura Y, Senda M, Iwasaki Y, Matoba N, Tamaki N, et al. PET and the autoradiographic method with continuous inhalation of oxygen-15-gas: theoretical analysis and comparison with conventional steady-state methods. J Nucl Med. 1993; 34:1672–80.
12. Hatazawa J, Fujita H, Kanno I, Satoh T, Iida H, Miura S, et al. Regional cerebral blood flow, blood volume, oxygen extraction fraction, and oxygen utilization rate in normal volunteers measured by the autoradiographic technique and the single breath inhalation method. Ann Nucl Med. 1995;9:15–21.
13. Shidahara M, Watabe H, Kim KM, Oka H, Sago M, Hayashi T, et al. Evaluation of a commercial PET tomograph-based system for the quantitative assessment of rCBF, rOEF and rCMRO2 by using sequential administration of ^{15}O-labeled compounds. Ann Nucl Med. 2002;16(5):317–27.
14. Hattori N, Bergsneider M, Wu HM, Glenn TC, Vespa PM, Hovda DA, et al. Accuracy of a method using short inhalation of 15O–O2 for measuring cerebral oxygen extraction fraction with PET in healthy humans. J Nucl Med. 2004;45:765–70.
15. Kudomi N, Hayashi T, Teramoto N, Watabe H, Kawachi N, Ohta Y, et al. Rapid quantitative measurement of $CMRO_2$ and CBF by dual administration ^{15}O-labeled oxygen and water during a single PET scan—a validation study and error analysis in anesthetized monkeys. J Cereb Blood Flow Metab. 2005;25:1209–24.
16. Kudomi N, Watabe H, Hayashi T, Iida H. Separation of input function for rapid measurement of quantitative $CMRO_2$ and CBF in a single PET scan with a dual tracer administration method. Phys Med Biol. 2007;52(7):1893–908.
17. Kudomi N, Choi E, Yamamoto S, Watabe H, Kim KM, Shidahara M, et al. Development of a GSO Detector Assembly for a Continuous Blood Sampling System. IEEE Trans Nucl Sci. 2003; 50(1):70–3.
18. Carson RE. Parameter estimation in positron emission tomography. In: Phelps ME, Mazziotta JC, Schelbert HR, editors. Positron emission tomography and autoradiography. New York: Raven Press; 1986. p. 347–90.
19. Shidahra M, Watabe H, Kim KM, Kudomi N, Ito H, Iida H. Optimal scan time of oxygen-15-labeled gas inhalation autoradiographic method for measurement of cerebral oxygen extraction fraction and cerebral oxygen metabolic rate. Ann Nucl Med. 2008;22(8):667–75.
20. Ito H, Kanno I, Fukuda H. Human cerebral circulation: positron emission tomography studies. Ann Nucl Med. 2005;19(2):65–74.

NeuroImage xxx (2009) xxx–xxx

Contents lists available at ScienceDirect

NeuroImage

journal homepage: www.elsevier.com/locate/ynimg

Quantitative evaluation of changes in binding potential with a simplified reference tissue model and multiple injections of [^{11}C]raclopride

Yoko Ikoma [a,b,*], Hiroshi Watabe [a], Takuya Hayashi [a], Yoshinori Miyake [c], Noboru Teramoto [a], Kotaro Minato [b], Hidehiro Iida [a]

[a] Department of Investigative Radiology, National Cardiovascular Center Research Institute, Suita, Osaka, Japan
[b] Graduate School of Information Science, Nara Institute of Science and Technology, Ikoma, Nara, Japan
[c] Department of Radiology and Nuclear Medicine, National Cardiovascular Center Hospital, Suita, Osaka, Japan

ARTICLE INFO

Article history:
Received 20 February 2009
Revised 27 May 2009
Accepted 29 May 2009
Available online xxxx

Keywords:
Positron emission tomography
[^{11}C]raclopride
Dopamine D_2 receptor
Multiple injections
Binding potential

ABSTRACT

Positron emission tomography (PET) with [^{11}C]raclopride is widely used to investigate temporal changes in the dopamine D_2 receptor system attributed to the dopamine release. The simplified reference tissue model (SRTM) can be used to determine the binding potential (BP_{ND}) value using the time–activity curve (TAC) of the reference region as input function. However, in assessing temporal changes in BP_{ND} using the SRTM, multiple [^{11}C]raclopride PET scans are required, and a second scan must be performed after the disappearance of the [^{11}C]raclopride administered in the first scan. In this study, we have developed an extended multiple-injection SRTM to estimate the BP_{ND} change, from a single PET scan with multiple injections of [^{11}C]raclopride, and we have validated this approach by performing numerous simulations and studies on monkeys. In the computer simulations, TACs were generated for dual injections of [^{11}C]raclopride, in which binding conditions changed during the scans, and the BP_{ND} values before, and after, the second injection were estimated by the proposed method. As a result, the reduction in BP_{ND} was correlated, either with the integral of released dopamine, or with the administered mass of raclopride. This method was applied to studies on monkeys, and was capable of determining two identical BP_{ND} values when there were no changes in binding conditions. The BP_{ND} after the second injection decreased when binding conditions changed due to an increase in administered raclopride. An advantage of the proposed method is the shortened scan period for the quantitative assessment of the BP_{ND} change for neurotransmitter competition studies.

Introduction

Neuroreceptor imaging using positron emission tomography (PET) and [^{11}C]raclopride has made it possible to determine the density of striatal dopamine D_2 receptors *in vivo* (Farde et al., 1985; Köhler et al., 1985; Hall et al., 1988). The binding potential ($BP_{ND} = k_3/k_4$) derived from rate constants in a two-tissue compartment model has been used to quantify the receptor binding (Mintun et al., 1984). Endres et al. then developed an extended compartment model, which included the released neurotransmitter concentration, and demonstrated that [^{11}C]raclopride binding decreased after the administration of amphetamine, which resulted in the displacement of the raclopride due to competition with increased dopamine (Endres et al., 1997. Carson et al., 1997). The model showed that the change in BP_{ND} between the baseline and the stimulated state was related to the total amount of released dopamine. Applying this theory, it has been shown that amphetamine-related reductions in [^{11}C]raclopride-specific binding in patients with schizophrenia was significantly greater than in healthy volunteers (Breier et al., 1997) and that a reduction in [^{11}C]raclopride binding was observed while playing a video game which resulted in the release of endogenous dopamine (Koepp et al., 1998). In this competition paradigm, two PET studies are necessary to measure the BP_{ND} values of the baseline and competed conditions, and a long study period is required.

On the other hand, single-scan studies with bolus-plus-continuous infusion (B/I) of the tracer, applied for the measurement of reduction in BP_{ND} due to an amphetamine challenge, were also performed (Carson et al., 1997, Endres et al., 1997). In these studies, a stimulus was administered during infusion of the tracer, and the change in binding between pre- and post-amphetamine intervention was measured as the tissue-to-plasma concentration ratio at equilibrium. This method enables the direct measurement of receptor-binding

* Corresponding author. Department of Investigative Radiology, National Cardiovascular Center Research Institute, 5-7-1, Fujishirodai, Suita, Osaka, 565-8565, Japan. Fax: +81 6 6835 5429.
E-mail address: ikoma@ri.ncvc.go.jp (Y. Ikoma).

1053-8119/$ – see front matter
doi:10.1016/j.neuroimage.2009.05.099

Please cite this article as: Ikoma, Y., et al., Quantitative evaluation of changes in binding potential with a simplified reference tissue model and multiple injections of [^{11}C]raclopride, NeuroImage (2009), doi:10.1016/j.neuroimage.2009.05.099

changes in a single scan. However, the design of the protocol requires that the tracer kinetics attain equilibrium within the measurement period of the pre- and post-amphetamine challenges (Watabe et al., 2000), and dynamic data that does not reach equilibrium may cause systematic errors in the estimates of binding changes (Zhou et al., 2006).

To compute the BP_{ND} value, the simplified reference tissue model (SRTM) is often used. The SRTM can provide the BP_{ND} without invasive arterial blood sampling by using a time–activity curve (TAC) of the reference region where specific bindings are negligible (Lammertsma and Hume, 1996). Recently, an extended simplified reference tissue model (ESRTM) was developed in order to quantify the reduction in BP_{ND} with B/I administration (Zhou et al., 2006). In the ESRTM method, the BP_{ND} of the SRTM was estimated separately, before and after, the pharmacological challenge during a 90 min scan with B/I administration. The group reported that stimulus-induced BP_{ND} changes, obtained from equilibrium analysis in the non-equilibrium state, resulted in an underestimation of the reduction in BP_{ND}, and that this was significantly improved by using the ESRTM. Nonetheless, B/I administration requires the equipment to provide [^{11}C]raclopride constantly during the scan, and there are often technical problems.

Kim et al. (2006) developed a method to measure regional cerebral blood flow in pre- and post-pharmacological stress from a single session of single photon emission computed tomography (SPECT) scanning with dual injections of ^{123}I-iodoamphetamine. In their paper, they showed mathematical derivation for estimating CBF values from two conditions in a single session of SPECT study. By advancing their method, we have developed a method to detect changes in receptor binding using a single session of PET scanning in conjunction with multiple bolus injections of [^{11}C]raclopride synthesized once before the scan (Watabe et al., 2006). In our approach, the SRTM was extended to measure the BP_{ND} of each injection, and we validated this approach by performing numerous simulations and studies on monkeys using PET and [^{11}C]raclopride.

Methods

Theory

The simplified reference tissue model (SRTM) provides BP_{ND} without arterial blood sampling by eliminating the arterial plasma TAC arithmetically from model equations, by using the TAC of the reference region where specific bindings are negligible. The radioactivity concentration of the target region (C_t) is expressed as Eq. (1), using the radioactivity concentration in the reference region (C_r), under the assumption that the target and reference regions can be expressed using the one-tissue compartment model and that the ratios of K_1 and k_2 are equal between the target and reference regions (Lammertsma and Hume, 1996).

$$C_t(t) = R_1 C_r(t) + \left(k_2 - \frac{R_1 k_2}{1 + BP_{ND}}\right) e^{-\frac{k_2}{1+BP_{ND}}t} \circledcirc C_r(t) \quad R_1 = K_1 / K_1^r \tag{1}$$

where K_1 and k_2 are the rate constants for the transfer from plasma to the displaceable compartment in the target tissue and from the displaceable compartment to plasma, respectively, and K_1^r is the rate constant for the transfer from plasma to the reference tissue.

We have extended this SRTM to a multiple-injection study. In this approach, the first injection of the radioligand was performed at the time of the scan start, and the BP_{ND} was measured as a baseline. Next, a second injection was performed simultaneously with a change in binding conditions, and the BP_{ND} was measured as a competitive state after the second injection. The BP_{ND} values before, and after, the second injection, were estimated by the multiple-injection simplified reference tissue model (MI-SRTM) expressed as follows:

$$\begin{aligned} C_{t1}(t) &= R_{11} C_{r1}(t) + \left(k_{21} - \frac{R_{11} k_{21}}{1 + BP_{ND1}}\right) e^{-\frac{k_{21}}{1+BP_{ND1}}t} \circledcirc C_{r1}(t) \\ C_{t2}(t) &= R_{12} C_{r2}(t) + \left(k_{22} - \frac{R_{12} k_{22}}{1 + BP_{ND2}}\right) e^{-\frac{k_{22}}{1+BP_{ND2}}t} \circledcirc C_{r2}(t) \\ &\quad + (C_{t0} - R_{12} C_{r0}) e^{-\frac{k_{22}}{1+BP_{ND2}}t} \end{aligned} \tag{2}$$

where C_{t1} and C_{t2} are the radioactivity concentrations in the target tissue and C_{r1} and C_{r2} are the radioactivity concentrations in the reference tissue for the first and second injections, respectively; t is the time from the first or second injection; C_{t0} and C_{r0} are the radioactivity concentrations of the target and reference tissues at the time of the second injection, respectively.

Firstly, R_{11}, k_{21} and BP_{ND1} were estimated by nonlinear least squares fitting with the iteration of the Gauss–Newton algorithm using data points before the second injection. Next, C_{r0} was calculated by the interpolation of the measured reference TAC, and C_{t0} was estimated using Eq. (1) with estimated R_{11}, k_{21} and BP_{ND1} values. Finally, R_{12}, k_{22}, and BP_{ND2} were estimated by nonlinear least squares fitting using these C_{r0} and C_{t0} values with Eq. (2). In this study using [^{11}C]raclopride, the TAC of the cerebellum was used as a reference TAC.

The present method can be used to generate voxel-based parametric maps. In the voxel-based estimation for parametric imaging of ligand–receptor binding, R_{11}, k_{21} and BP_{ND1} from the first injection and R_{12}, k_{22}, and BP_{ND2} from the second injection in Eq. (2), were estimated by a basis function method in which the model Eq. (2) is solved using linear least squares for a set of basis functions, which enables the incorporation of parameter bounds (Gunn et al., 1997).

Simulation analysis

Three simulation studies were carried out to validate the present approach and to determine: 1) whether the change in BP_{ND} caused by competition to receptor binding could be detected by the MI-SRTM; 2) how would the time delay between the endogenous dopamine release and [^{11}C]raclopride injection affect BP_{ND} estimates, and 3) what was an optimal scan duration for a reliable BP_{ND} estimation?

Detection of BP_{ND} change with dual injections

The MI-SRTM assumes that BP_{ND} alters promptly from BP_{ND1} to BP_{ND2} at the time of the second injection and then remains constant. However, in reality this is unlikely and the binding condition of [^{11}C]raclopride may be continuously changed along time. In this simulation, the detectability of the reduction of BP_{ND} due to changes in binding conditions was investigated. Noiseless time–activity curves of the striatum and cerebellum were generated with a measured plasma TAC and assumed parameter values derived from measurements taken from the monkey study. A TAC of the cerebellum was simulated with a conventional two-tissue compartment, four-parameter model with assumed parameter values obtained previously in our monkey study: $K_1 = 0.034$, $K_1/k_2 = 0.36$, $k_3 = 0.022$, $k_4 = 0.034$. Meanwhile, a TAC of the striatum was simulated with an extended two-tissue compartment model

Please cite this article as: Ikoma, Y., et al., Quantitative evaluation of changes in binding potential with a simplified reference tissue model and multiple injections of [^{11}C]raclopride, NeuroImage (2009), doi:10.1016/j.neuroimage.2009.05.099

expressed as Eq. (3) by the fourth-order Runge–Kutta method (Endres et al., 1997).

$$\begin{aligned}
\frac{dC_f}{dt} &= K_1 C_p(t) - (k_2 + k'_3(t))C_f(t) + k_4 C_b(t) \\
\frac{dC_b}{dt} &= k'_3(t)C_f(t) - k_4 C_b(t) \\
k'_3(t) &= k_{on}\frac{B_{max} - \frac{C_b(t)}{SA}}{1 + D(t)} \\
D(t) &= B_1 \qquad (t<t_2) \\
&= B_2 + A\cdot\exp(-R(t-t_2)) \quad (t\geq t_2)
\end{aligned} \tag{3}$$

where C_f and C_b are the concentrations of radioactivity for free and specifically bound [^{11}C]raclopride in tissue, respectively; B_{max} is the total dopamine D_2 receptor concentration; k_{on} is the bimolecular association rate constant for raclopride; SA is the specific activity of administered [^{11}C]raclopride; D is the concentration of free dopamine. In this simulation study, t_2 was set to 30 min, and SA that was decay corrected to the first injection time was assumed to be equal in first and second injections with a single synthesis. Each assumed parameter for K_1 to k_4 was obtained from our monkey study, and the B_{max} value was as reported previously (Endres et al., 1997), thus $K_1 = 0.033$, $K_1/k_2 = 0.59$, $k_{on} = 0.0048$, $B_{max} = 17.6$; $k_4 = 0.026$; $B_1 = B_2 = 0$, and SA = 37 GBq/μmol at the time of first injection.

First, the magnitude of the BP_{ND} change, derived from an increase in released dopamine, was investigated. Time–activity curves, including dopamine release, were simulated from Eq. (3), in which A varied: 0.5, 1.0, 1.5 and 2.0, and R varied: 0.04, 0.07, and 0.1. In these simulated TACs, BP_{ND1} and BP_{ND2} were estimated by the MI-SRTM, and the relationship between the magnitude of the BP reduction ($\Delta BP = (BP_{ND1} - BP_{ND2})/BP_{ND1}$) and the integral of the dopamine pulse D in Eq. (3) was examined.

Next, the BP change caused by an increase in administered raclopride was investigated. $D(t)$ in Eq. (3) was set to 0, and tissue TACs were generated using the input plasma TAC in which administration of the first injection was assumed as 1 nmol raclopride, and the second injection was amplified from 1 to 50 times greater than the first injection. In these simulated TACs, BP_{ND1} and BP_{ND2} were estimated by the MI-SRTM, and the relationship between the magnitude of ΔBP and the amount of raclopride administered by the second injection was examined.

Effect of binding change timing on BP_{ND} estimates

It is possible that the change in BP_{ND} occurs either before, or after, the second injection of [^{11}C]raclopride. In the MI-SRTM, the error in the estimates for the first injection of [^{11}C]raclopride amplifies the errors in the estimates for the second injection. In this simulation, the effect of the onset of the dopamine pulse on the binding change of BP_{ND}, estimated by the MI-SRTM, was investigated using noiseless simulated TACs. First, TACs with a released dopamine pulse were generated using Eq. (3), with the parameters mentioned above, and three types of pulse ($A = 0.5$, $R = 0.1$; $A = 1.0$, $R = 0.07$; $A = 1.5$, $R = 0.04$) in which the onset time of the dopamine pulse, t_2 in Eq. (3), was changed from −10, −5, 0, 5, 10, 15 min against 30 min intervals of the second injection. The values for BP_{ND1}, BP_{ND2}, and ΔBP were estimated by the MI-SRTM, and the relationship between the onset time of the dopamine pulse and the BP_{ND} estimates was investigated.

Next, TACs were generated by the SRTM with measured cerebellum TACs and assumed parameter values ($R_1 = 0.86$, $k_2 = 0.091$, and $BP_{ND1} = 2.2$) using the fourth-order Runge–Kutta method, assuming a prompt change of BP_{ND} at −10, −5, 0, 5 and 10 min after the second injection (30 min intervals). The value of BP_{ND2} was also varied so that ΔBP would be 0, 10, 20, 30, 40, 50, 60, 70, and 80%. In these simulated TACs, BP_{ND1}, BP_{ND2}, and ΔBP were estimated by the MI-SRTM, and the estimated values were compared with the true values.

Effect of injection interval on BP_{ND} estimates

The relationship between the reliability of the BP_{ND} estimates from the MI-SRTM and the injection interval was investigated with noise-added TACs. A dynamic tracer concentration for [^{11}C]raclopride was derived from the equation of MI-SRTM (Eq. (2)) with a measured cerebellum TAC used as the input function and the rate constant values given as true values ($R_1 = 0.95$, $k_2 = 0.067$, $BP_{ND1} = 2.6$, $BP_{ND2} = 2.6$, 1.8, or 0.78) assuming a prompt BP reduction at the time of the second injection. The timing of the second injection was varied from 20 min to 90 min after the first scan.

The Gaussian-distributed mean-zero noise with variance proportional to the true count was added to the non-decaying tissue activity for each frame using Eq. (4) (Logan et al., 2001):

$$\sigma_i(\%) = 100\cdot F/\sqrt{C_t(t_i)\cdot e^{-\lambda t_i}\cdot \Delta t_i} \tag{4}$$

where i is the frame number; C_t is the non-decaying tissue radioactivity concentration derived from the rate constants and the input function; t_i is the midpoint time of the i'th frame; Δt_i is the data collection time; λ is the radioisotope decay constant; F is a scaling factor representing the sensitivity of the measurement system, introduced here to adjust the noise level. It should be noted that this equation assumes that noise, which is added to the TAC, is determined by the count of the curve itself. In fact, noise is determined by the total counts in the slice, and is affected by random counts, dead time, etc. In this simulation study, F was set to 15.0 so that the noise level would be the same as the noise level for regions of interest (ROI)-based analysis, and 1000 noisy data sets were generated for each injection interval.

In these simulated TACs, BP_{ND1} and BP_{ND2} were estimated by the MI-SRTM, and estimated BP_{ND1}, BP_{ND2}, and ΔBP values were compared with the true values. Parameter estimates were considered outliers if either BP_{ND1} or BP_{ND2} was outside the range $0.0 < BP_{ND} < 10.0$. The reliability of the estimated parameters was evaluated by the mean and coefficient of variation (COV; SD/mean[%]) of the estimates excluding outliers, and the relationship between the reliability of the parameter estimates and the injection interval was investigated.

Monkey study analysis

Studies on monkeys with dual injections of [^{11}C]raclopride were performed to determine whether the present approach can estimate two identical BP_{ND} values when there is no change in binding conditions during the scan, and whether this approach can detect a change in BP_{ND} values when the binding conditions do change during the scan. The monkeys were maintained and handled in accordance with guidelines for animal research on Human Care and Use of Laboratory Animals (Rockville, National Institute of Health/Office for Protection from Research Risks, 1996). The study protocol was approved by the Subcommittee for Laboratory Animal Welfare of the National Cardiovascular Center.

First, PET studies were performed in four cynomolgus macaques (weight 3.6 ± 0.56 kg) by administering the same molar amount of [^{11}C]raclopride for the first and second injections (Table 1). Anesthesia was induced with ketamine (8.4 mg/kg, intramuscularly) and xylazine (1.7 mg/kg, intramuscularly) and maintained by intravenous propofol (6 mg/kg/h) and vecuronium (0.02 mg/kg/h) during the scan. Initially, 418 ± 111 MBq of [^{11}C]raclopride was administered by a bolus injection, and after 30 min, the same molar amount of [^{11}C] raclopride as for the first injection, was administered by a bolus

Please cite this article as: Ikoma, Y., et al., Quantitative evaluation of changes in binding potential with a simplified reference tissue model and multiple injections of [^{11}C]raclopride, NeuroImage (2009), doi:10.1016/j.neuroimage.2009.05.099

Table 1
Injection protocol in monkey studies with dual injections of [^{11}C]raclopride.

	Subject	Specific activity at the time of first injection [GBq/μmol]	Injection interval [min]	First injection		Second injection	
				Injected mass [nmol]	Injected activity at the time of first injection [MBq]	Injected mass [nmol]	Injected activity at the time of second injection [MBq]
	#1	64.9	30	8.4	548		198
	#2	75.2	30	5.9	444		160
Exp. 1	#3	29.3	30	13.6	399	Same as first injection	144
	#4	39.7	30	7.1	280		101
	mean ± SD	52.3 ± 21.4	30	8.8 ± 3.4	418 ± 111		151 ± 39.9
Exp. 2	#5	22.6	30	3.3	73.3	30.7	249

Exp. 1: Dual injections with same mass of [^{11}C]raclopride.
Exp. 2: Dual injections with different mass of [^{11}C]raclopride.

injection. Data were acquired for 60 min (10 s × 18, 30 s × 6, 120 s × 7, 300 s × 2 for the first injection; 10 s × 18, 30 s × 6, 120 s × 7, 300 s × 2 for the second injection). The specific radioactivity was 52.3 ± 21.4 GBq/μmol at the time of the first injection.

Next, PET studies were performed on a cynomolgus macaque (weight 6.0 kg) with the administration of different molar amounts of [^{11}C]raclopride for the first and second injections by changing the volume of second injection with [^{11}C]raclopride which was synthesized before the first injection (Table 1). For the first injection, a bolus of 73.3 MBq of [^{11}C]raclopride, (3.3 nmol of raclopride) was administered, and after 30 min, 249 MBq at the time of the second injection (decay corrected 691MBq) of [^{11}C]raclopride (30.7 nmol of raclopride) was administered by bolus injection. The specific radioactivity was 23 GBq/μmol at the time of the first injection.

PET scans were performed using a PCA-2000A positron scanner (Toshiba Medical Systems Corporation, Tochigi, JAPAN) that provides 47 planes and a 16.2 cm axial field of view. A transmission scan with a 3-rod source of ^{68}Ge–^{68}Ga was carried out for 20 min for attenuation correction before the administration of [^{11}C]raclopride. Radioactivity was measured in two-dimensional mode and the data were reconstructed by a filtered back-projection using a Gaussian filter (full width at half maximum is about 6.0 mm (Herzog et al., 2004)). VOIs were defined manually over the left and right striatum and cerebellum for PET images, and the radioactivity concentration in these regions was obtained. For each region, R_{11}, k_{21}, BP_{ND1}, R_{12}, k_{22}, and BP_{ND2} were estimated by MI-SRTM. In addition, parametric images were generated, estimating each parameter voxel by voxel, using the MI-SRTM with the basis function method.

Results

Detection of BP_{ND} change with dual-injection

Typical examples of simulated TACs in the dual-injection study with dopamine release are shown in Fig. 1. In the simulation studies, the magnitude of ΔBP, estimated by the MI-SRTM, was investigated in the two cases where the specific binding changed due to the released dopamine pulse or to an increase in administered raclopride. The magnitude of ΔBP increased as the integral of the dopamine pulse increased (Fig. 2A). To some extent there was a good linear correlation between the reduction in BP_{ND} and the integral of the dopamine pulse ($Y = 2.0*X + 2.3$, $R^2 = 0.95$ where $X < 15$ (X: Integral of the dopamine pulse, Y: reduction in BP_{ND})); however the relationship did not remain linear for a large dopamine pulse. The reduction in BP_{ND} also became greater when the injected mass of raclopride increased, although its relationship was nonlinear (Fig. 2B).

Effect of binding change timing on BP_{ND} estimates

In the simulation with a released dopamine pulse, when the dopamine pulse was released before the second injection, the BP_{ND1} value was underestimated and BP_{ND2} was overestimated, compared with the situation where the dopamine pulse was released at the same time as the second injection (Figs. 3A, B). On the other hand, when the dopamine pulse was released after the second injection, BP_{ND1} was unchanged and BP_{ND2} varied according to the onset and magnitude of the dopamine pulse. The reduction in BP_{ND} also depended on the

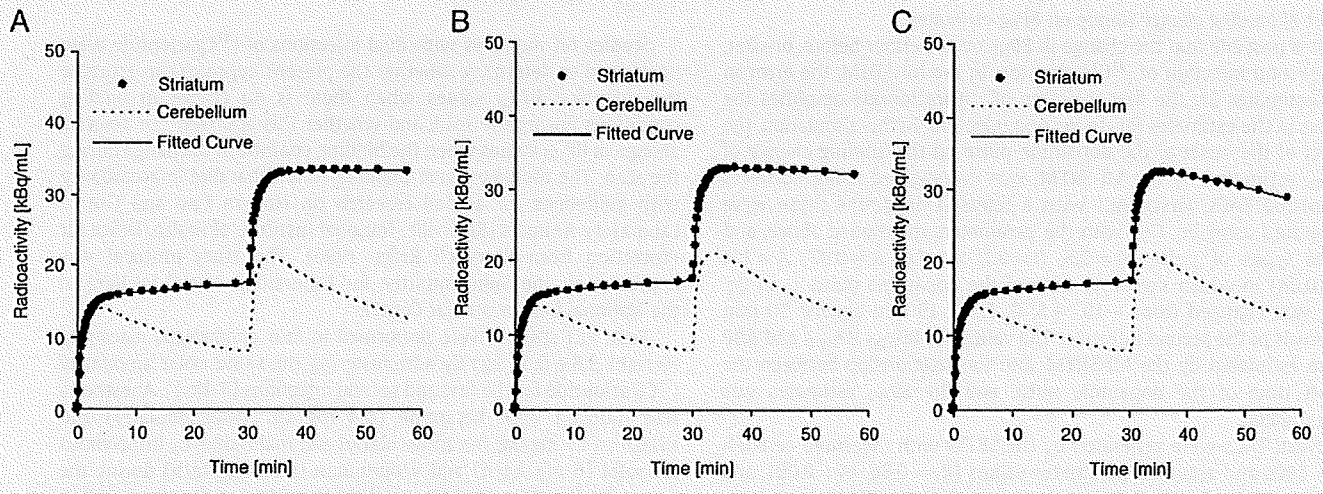

Fig. 1. Simulated time-activity curves for the striatum and cerebellum without dopamine pulse (A), with small dopamine pulse ($A = 0.5$, $R = 0.04$) (B), and with large dopamine pulse ($A = 1.5$, $R = 0.1$) (C), and fitted curve for the striatum by MI-SRTM.

Please cite this article as: Ikoma, Y., et al., Quantitative evaluation of changes in binding potential with a simplified reference tissue model and multiple injections of [^{11}C]raclopride, NeuroImage (2009), doi:10.1016/j.neuroimage.2009.05.099

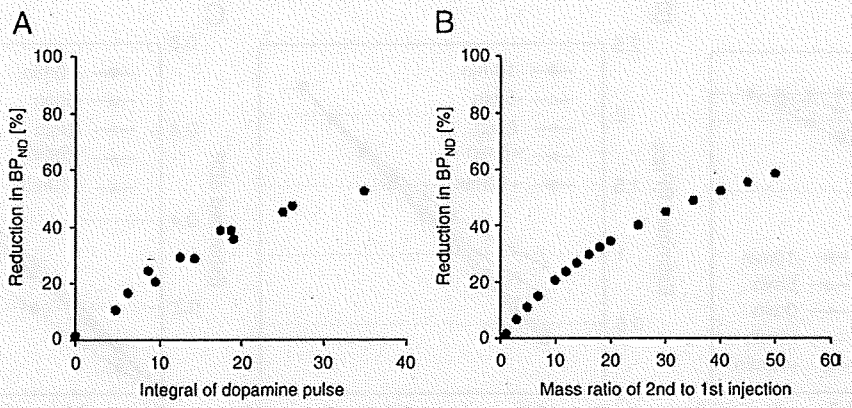

Fig. 2. Relationship between percentage reduction in BP_{ND} and the integral of the dopamine pulse in simulation studies in which dopamine was released at the same time as the second injection, performed 30 min after first injection (A); and the relationship between percentage reduction in BP_{ND} and the mass of the second injection in simulation studies in which a greater mass of raclopride was administered 30 min after the first injection.

onset, magnitude of amplitude, and decay rate of the dopamine pulse, and the reduction in BP_{ND} was greatest when the dopamine pulse was released 5 min after the second injection (Fig. 3C). When the magnitude of the dopamine pulse was small, the detected BP_{ND} reduction was small when the dopamine pulse was released before the second injection, becoming greatest (about 20%) when the pulse was released 5 min or 10 min after the second injection. When the magnitude of the pulse was medium, the BP_{ND} reduction was 20% when the pulse was released 5 min before the second injection, and it was greatest (about 35%) when the pulse was released 5 min after the second injection. When the dopamine pulse was large, the detected BP_{ND} reduction was 30% even when the pulse was released 10 min before the second injection, and was greatest (about 45%) when the pulse was released 0 or 5 min after the second injection.

In the simulation with prompt BP_{ND} reduction, BP_{ND1}, BP_{ND2} and ΔBP were estimated precisely by the MI-SRTM when the BP_{ND} reduction occurred at 30 min, in other words, at the same time as the second injection (Fig. 4). In the case where the BP decreased before 30 min, the estimated BP_{ND1} was lower than the true value for BP_{ND1} (=2.2), and the magnitude of the underestimation increased when the true BP_{ND2} was lower, that is to say, the reduction in BP_{ND} was greater (Fig. 4A). There were slight errors in BP_{ND2} estimates (Fig. 4B). When the BP_{ND} decreased 50% (BP_{ND1} = 2.2 and BP_{ND2} = 1.1) at 10 min before the second injection, estimated BP_{ND1} was 1.63 and BP_{ND2} was 1.04. Conversely, when the BP decreased after 30 min, BP_{ND1} was estimated precisely, and BP_{ND2} was overestimated (Figs. 4A and B). The error in BP_{ND2} estimates increased as the magnitude of the BP_{ND} reduction increased. When the BP_{ND} decreased 50% (BP_{ND1} = 2.2 and BP_{ND2} = 1.1) at 10 min after the second injection, estimated BP_{ND1} was 2.20 and BP_{ND2} was 1.28. With respect to the magnitude of the BP reduction, the estimated ΔBP was lower than the true value when the BP reduction was greater, or the difference between the timing of the BP_{ND} decrease and the second injection was greater (Fig. 4C). When the BP_{ND} reduction began 10 min before the second injection, the error in the estimated ΔBP was considerable. However, when the BP_{ND} reduction began, either 5 min before or 5 min after, the second injection, the error in ΔBP was less than 5% when the reduction in the BP was lower than 50%.

Effect of injection interval on BP_{ND} estimates

Errors in the estimated BP_{ND1}, BP_{ND2} and ΔBP values were investigated in simulated noise-added TACs for various injection intervals, and it was observed that the errors became larger as the injection interval became shorter (Fig. 5). The COVs of BP_{ND1} and BP_{ND2} were less than 5% and the bias was less than 1% when the injection interval was longer than 30 min, in both cases where the reduction in the BP_{ND} was 30% and 70%. When ΔBP was 30%, the bias increased suddenly, and the COV of ΔBP rose to over 10% for an injection interval of less than 40 min. There were no outliers even if the injection interval was 20 min. Meanwhile, when ΔBP was 70%, there was little bias and the COV of ΔBP was less than 10% for an injection interval longer than 30 min. The COV of ΔBP in the 70% reduction TAC was lower than that in 30% reduction TAC. However,

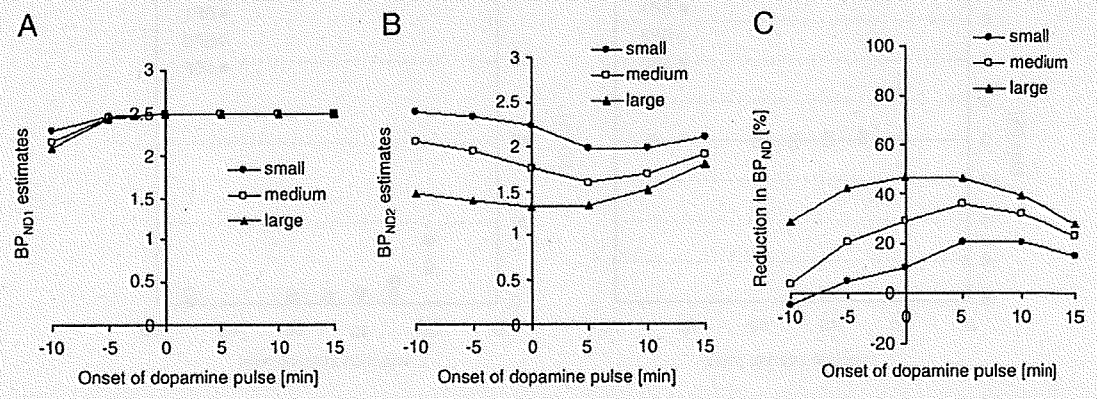

Fig. 3. Relationship between estimated values of BP_{ND1} (A), BP_{ND2} (B), reduction in BP_{ND} (C) and the onset of the dopamine pulse, in simulation studies with a small pulse (H = 0.5, R = 0.1), medium pulse (H = 1.0, R = 0.07), and large pulse (H = 1.5, R = 0.04) released −10, −5, 0, +5, +10, or +15 min with respect to the second injection.

Please cite this article as: Ikoma, Y., et al., Quantitative evaluation of changes in binding potential with a simplified reference tissue model and multiple injections of [^{11}C]raclopride, NeuroImage (2009), doi:10.1016/j.neuroimage.2009.05.099

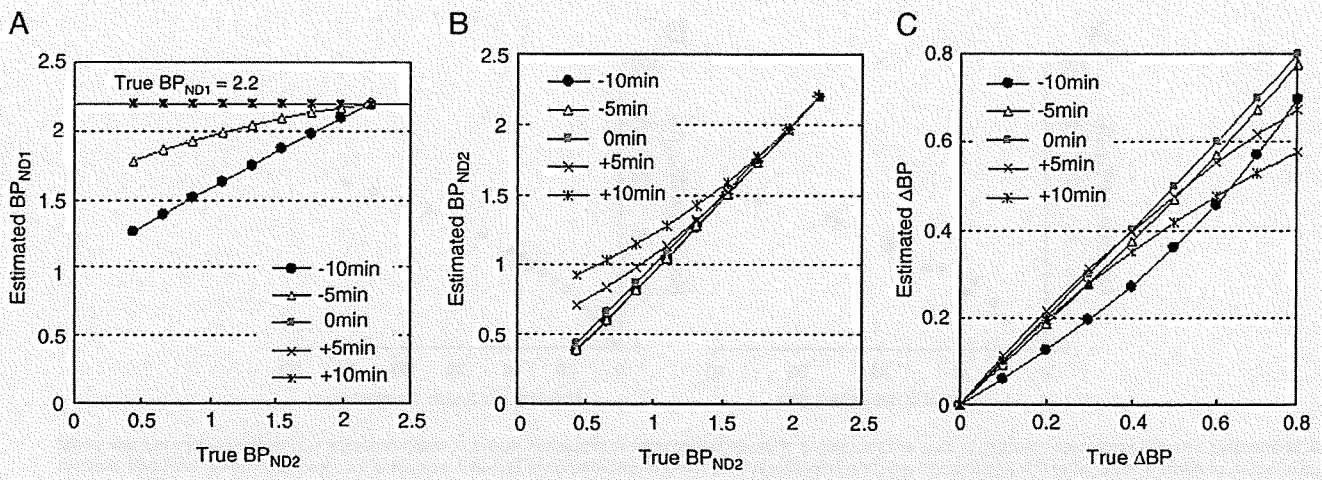

Fig. 4. Relationship between estimated values of BP_{ND1} (A), and BP_{ND2} (B) and the true values of BP_{ND2}, and the relationship between the estimated reduction in BP_{ND} (ΔBP) and true ΔBP (C) in the simulation studies in which BP_{ND} changed promptly from 2.2 to the true BP_{ND2} at −10, −5, 0, +5, or +10 min, with respect to the second injection.

there were 22 outliers with unreasonable estimates when the injection interval was 20 min and one outlier in one thousand estimates when the injection interval was 30 min.

Monkey studies

Typical examples of TACs for the striatum and the cerebellum in the dual-injection study with the same amount of raclopride are shown in Fig. 6. In these studies, the BP_{ND} values for the first and second injections could be estimated, and there were little differences between BP_{ND1} and BP_{ND2} (Table 2).

Time–activity curves for the striatum and the cerebellum in the dual-injection study using different amounts of raclopride are shown in Fig. 7, and the parametric images of BP_{ND1} and BP_{ND2} are shown in Fig. 8. The estimated BP decreased when the binding changed at the second injection due to the addition of more raclopride than was

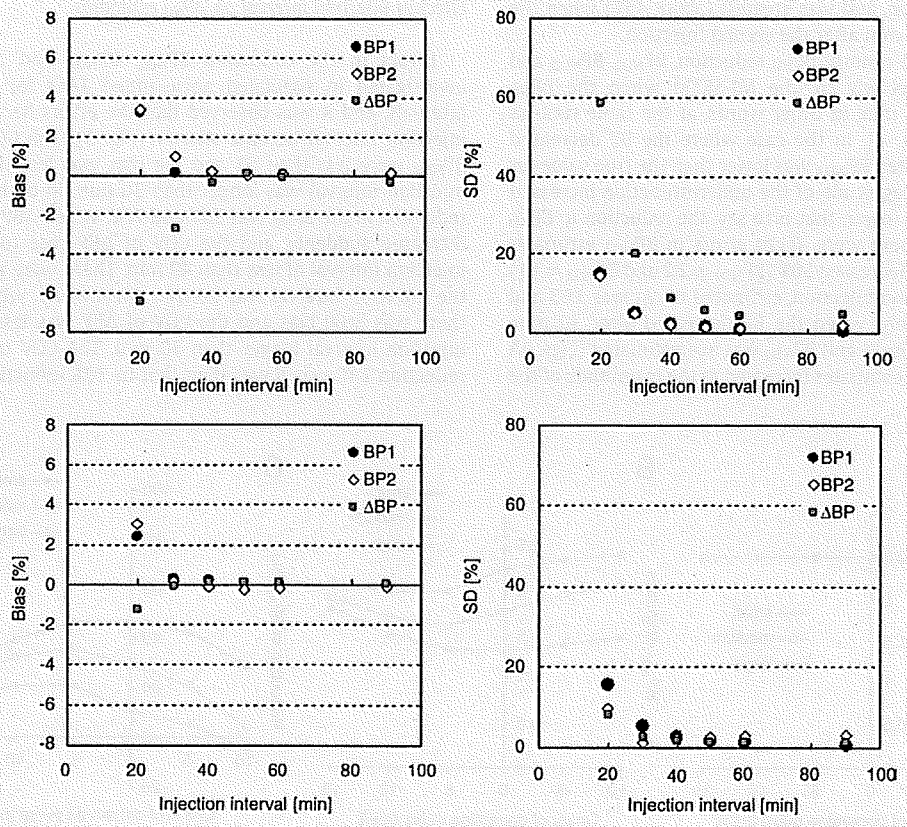

Fig. 5. Relationship between the injection interval and bias (left) or SD (right) of BP_{ND1}, BP_{ND2}, and the reduction in BP_{ND} (ΔBP) when BP_{ND} decreased by 30% (upper) or 70% (lower) at the time of second injection.

Please cite this article as: Ikoma, Y., et al., Quantitative evaluation of changes in binding potential with a simplified reference tissue model and multiple injections of [^{11}C]raclopride, NeuroImage (2009), doi:10.1016/j.neuroimage.2009.05.099

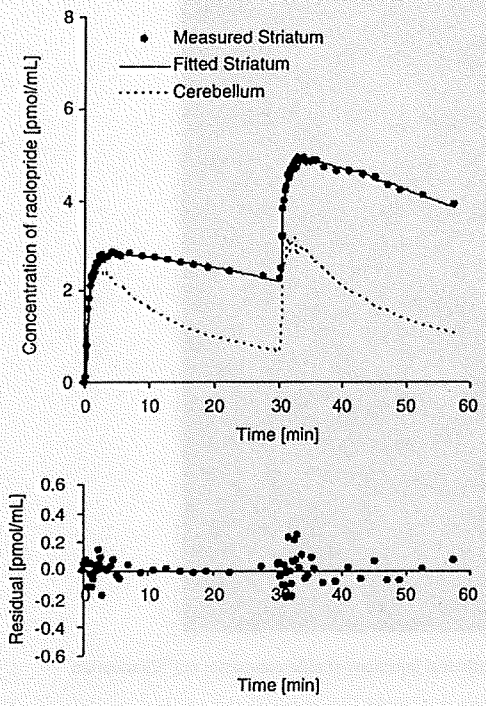

Fig. 6. Measured time–activity curves of the striatum and cerebellum in the dual-injection study with the same mass of [^{11}C]raclopride and a fitted curve for the striatum, using the multiple-injection SRTM (upper), and residuals between measured and fitted curves (lower).

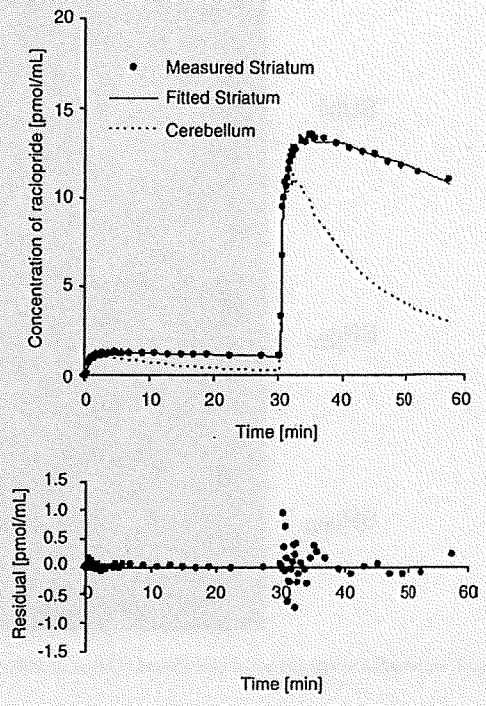

Fig. 7. Measured time–activity curves of the striatum and cerebellum in the dual-injection study with a different mass of [^{11}C]raclopride and a fitted curve for the striatum, using the multiple-injection SRTM (upper), and residuals between measured and fitted curves (lower).

administered for the first injection. Estimated BP_{ND1}, BP_{ND2} and ΔBP values in the striatum were 2.7, 2.0, and 25%, respectively (Table 2). The reduction in BP_{ND} was also observed in the parametric images as shown in Fig. 8.

Discussion

In the competition paradigm, the binding potential of [^{11}C] raclopride reflects the condition of specific binding to dopamine D_2 receptors, which is affected by competition with other ligands if there are no changes in the density of the receptors. The SRTM can provide the BP_{ND} value without invasive arterial blood sampling, using a TAC of the reference region, where specific bindings are negligible (Lammertsma and Hume, 1996), and this method has been widely used to estimate the binding of neuroreceptor ligands. However, in assessing temporal changes in the BP_{ND} of the SRTM caused by competition for receptor binding due to pharmacological administration or cognitive activation, multiple [^{11}C]raclopride PET scans are necessary and a long study period is required. To overcome this complication, we have proposed a multiple-injection approach in which the temporal change in BP_{ND} is quantified in a single scan with multiple [^{11}C]raclopride injections. This approach takes into account the residual radioactivity from the first injection in the target tissue, at the time of the second injection, as the initial condition in Eq. (2), and makes it possible to perform the second injection immediately, following data acquisition from the first injection. Thus it is possible to determine the change in BP_{ND} from a short study period.

There have been several investigators who attempted to perform multiple injections of ligands with PET studies for either obtaining receptor density and affinity by changing specific activity (Delforge et al., 1995; Millet et al., 1995; Morris et al., 1996a,b; Muzic et al., 1996; Christian et al., 2004; Gallezot et al., 2008), or obtaining different kinetic parameters simultaneously by injecting different tracers such as [^{11}C]flumazenil and [^{18}F]FDG (Ikoma et al., 2004; Koeppe et al., 2001). MI-SRTM gives us alternative approach for multiple-injection study which is aimed at shortening study period.

Table 2
Estimated BP_{ND1}, BP_{ND2}, and difference between BP_{ND1} and BP_{ND2} in monkey studies with dual injections of [^{11}C]raclopride.

	Subject	BP_{ND1}	BP_{ND2}	ΔBP
	#1	1.86	2.15	0.15
	#2	1.98	2.01	0.014
Exp. 1	#3	1.95	1.79	−0.081
	#4	2.33	2.39	0.027
	mean ± SD	2.03 ± 0.20	2.08 ± 0.25	0.029 ± 0.097
Exp. 2	#5	2.66	2.00	−0.25

$\Delta BP = (BP_{ND2} - BP_{ND1}) / BP_{ND1}$.
Exp. 1: Dual injections with same mass of [^{11}C]raclopride.
Exp. 2: Dual injections with different mass of [^{11}C]raclopride.

Detection of binding changes with the SRTM

In the multiple-injection approach, it is assumed that the change in binding conditions is reflected by a reduction in BP_{ND} estimated from the SRTM. The analysis method based on the compartment model assumes that the rate constants of K_1 to k_4 are constant during the scan. However, in studies with changes in binding conditions, levels of endogenous dopamine change after exposure to stimuli such as an amphetamine challenge (Endres et al., 1997; Laruelle et al., 1997), and the value of $k_3'(t)$ in Eq. (3) varies according to the concentration of free dopamine (Laruelle et al., 1997, Endres et al., 1997). Therefore, estimates of BP_{ND} following exposure to stimuli are considered to be an average value over time that is influenced by the dynamics of the neurotransmitter. However, it has been reported that reductions in BP_{ND}, estimated from graphical analysis or multilinear analysis, in simulation studies for two separate bolus-injection scans, are related to the integral of dopamine release (Endres and Carson, 1998; Yoder et al., 2004), and the reduction in BP_{ND} is a useful index for the evaluation of binding conditions in competition paradigms.

Please cite this article as: Ikoma, Y., et al., Quantitative evaluation of changes in binding potential with a simplified reference tissue model and multiple injections of [^{11}C]raclopride, NeuroImage (2009), doi:10.1016/j.neuroimage.2009.05.099

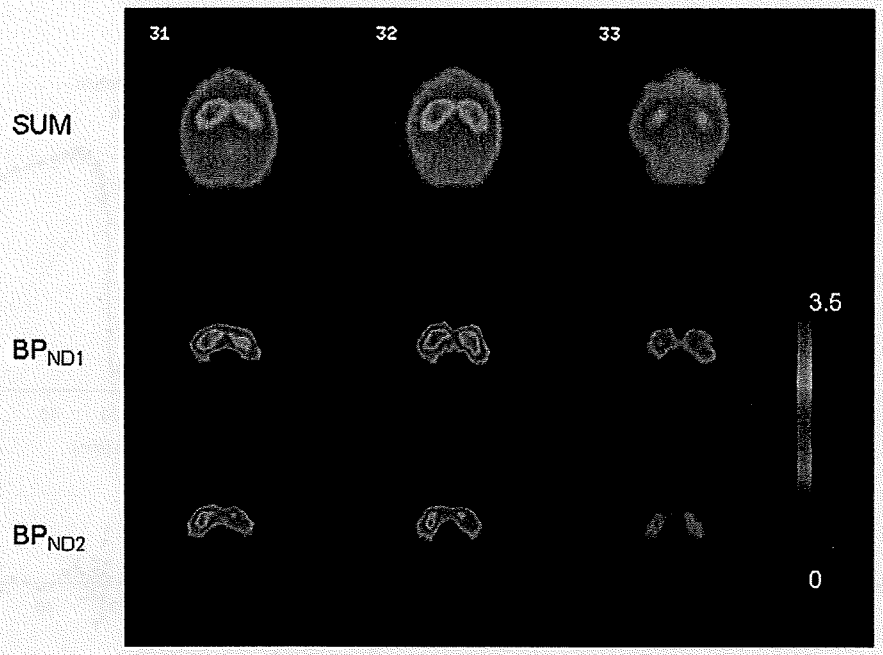

Fig. 8. Summation image and parametric images of BP_{ND1} and BP_{ND2} in the monkey study with dual injections of different masses of [^{11}C]raclopride.

In addition, in the SRTM, there are further assumptions that the target tissue and reference tissue can be expressed by a one-tissue compartment model, and the ratio of K_1 and k_2 are equal between the target and reference regions (Lammertsma and Hume, 1996). Strictly speaking, this assumption does not apply to [^{11}C]raclopride studies because significantly better fits were obtained with a two-tissue compartment model, as compared with those obtained with a one-tissue compartment model in cerebellum and striatum TACs (Lammertsma et al., 1996). Therefore, this assumption of the SRTM induces a bias in BP_{ND} estimates even in an ordinary single-injection study. In the MI-SRTM, which is an extension of the SRTM, the effect of the assumption could be more severe than for the SRTM because the bias in BP_{ND1} could be propagated to the estimation of BP_{ND2}. However, in our simulation studies, the ΔBP_{ND}, estimated from the MI-SRTM, increased according to the increase in the dopamine pulse or to administered raclopride (Fig. 2). When the specific binding of administered [^{11}C]raclopride competed with that of endogenous dopamine, to some extent the reduction in BP increased in proportion to the integral of the released dopamine pulse, and approached saturation as the integral of the pulse increased. This is consistent with results reported in previous studies (Endres and Carson, 1998, Yoder et al., 2004). Furthermore, in the monkey studies, it was confirmed that there was little change in BP_{ND} when the same mass of raclopride was administered for the first and second injections (Fig. 6), and the BP_{ND} decreased in accordance with the increase in administered raclopride (Figs. 7 and 8). Morris et al. (1996b) intensively investigated the characteristics of multiple injections PET studies, and they showed varied specific activity by multiple injections introduced bias in estimates of kinetic parameters. Our results may be influenced by the abrupt discontinuity in mass of raclopride due to the second injection. However, the result of second monkey study (10 times higher mass in the second injection) agreed well with the simulation (Fig. 2B) although further validation studies will be needed to confirm this result.

Effect of binding change timing on BP_{ND} estimates

In estimating the BP_{ND} after the dopamine pulse release, the timing of the [^{11}C]raclopride injection has been shown to affect the BP_{ND} estimates (Yoder et al., 2004). In the simulation study of our multiple-injection approach, BP_{ND1} (in other words, the BP_{ND} for the condition without dopamine activation) had few errors, except when the dopamine pulse was released 10 min before the second injection. In these simulations, BP_{ND1} was estimated using the data from the time interval between the first injection and the second injection. Therefore, when the BP_{ND} reduction, due to an increase in free dopamine, started before the second injection, the value for BP_{ND1} was underestimated. However, this underestimation can be avoided by adjusting the data points used for the fitting of BP_{ND1} so that BP_{ND1} is determined before a change in the binding conditions. On the other hand, BP_{ND2}, (that is to say, the BP_{ND} of the condition with dopamine activation) was affected by the timing of the dopamine pulse release. The estimated BP_{ND2} decreased as the onset of the dopamine pulse occurred later, and was smallest when the dopamine pulse was released 5 min after the second injection. As a result, the magnitude of ΔBP was greatest when the dopamine pulse was released 5 min after the second injection.

The value of $k_3'(t)$ in Eq. (3) depends upon the amount of free dopamine at time t (Endres et al., 1997, Endres and Carson, 1998) and the released dopamine pulse decreases as time goes by. Therefore, if the specific activity of administered [^{11}C]raclopride is high enough, the time-varying binding potential ($BPs(t) = k_3'(t)/k_4$) is lowest at the time of the pulse release, and it becomes greater, and approaches the level before the pulse release, as time passes. Meanwhile, the reduction in BP_{ND} is determined by both the $BPs(t)$ and the concentration of free tracer (Endres and Carson, 1998). In the TACs from our simulation studies, the concentration of free [^{11}C]raclopride had a peak at about 5 min after the injection, and ΔBP_{ND} was greatest when the onset of the dopamine pulse occurred 5 min after the injection, as shown in Fig. 3C. Therefore, the reduction in BP_{ND} was greatly affected, not only by the magnitude of the dopamine pulse, but also by its timing. In other words, if the kinetics of the free tracer are similar, that is to say the value of k_2 does not change markedly, and the timing of the dopamine release is the same, the estimated ΔBP changes according to the integral of the dopamine pulse as shown in Fig. 2.

In the situation where BP_{ND} changed promptly, the ΔBP_{ND} also depends upon the magnitude and timing of the BP_{ND} reduction. However, when ΔBP_{ND} was less than 40% and the time difference

Please cite this article as: Ikoma, Y., et al., Quantitative evaluation of changes in binding potential with a simplified reference tissue model and multiple injections of [^{11}C]raclopride, NeuroImage (2009), doi:10.1016/j.neuroimage.2009.05.099

between the binding change and second injection was within 5 min, the effect of the timing of the BP_{ND} reduction was slight.

Interval between the dual injections

In the simulation study with noise for the ROI-based estimation, a dual-injection scan with a 30 min injection interval, gave unbiased and reliable BP_{ND1} and BP_{ND2} estimates (Fig. 5). In the 70% reduction TAC, the COV of ΔBP_{ND} was less than 5% when the injection interval was 30 min. Conversely, results from the 30% reduction TAC showed that a 50 min interval would be required to estimate ΔBP_{ND} within a 5% COV. In this study, we evaluated the reliability of BP_{ND} estimates for an ROI-based estimation. However, in voxel-based estimations, the noise level is usually higher, so the COV of estimates can be expected to increase.

In the ROI analysis of human study with single injection, it is reported that a 30 min scan of [^{11}C]raclopride gave unbiased and reliable BP_{ND} estimates (Ikoma et al., 2008). The kinetics of [^{11}C] raclopride in the human brain is different from that in the monkey brain, inducing the difference in required scan durations. The required injection interval for a reliable estimation depends on the kinetics of the ligand, the magnitude of ΔBP_{ND} and the noise level according to injection dose, ROI size, sensitivity of the measurement system, and so on. Therefore, evaluating the effect of the injection interval on the reliability of parameter estimates is important.

Monkey studies

In the simulation studies, it was demonstrated that the MI-SRTM approach could detect a change in BP_{ND} caused by the release of a dopamine pulse or by the increase in administered raclopride. Furthermore, we demonstrated the validity of the proposed method using actual data from monkeys. As a result, the estimated BP_{ND} reduction changed according to the injected mass of raclopride in the second injection, and this is consistent with the results from the simulation studies. We are planning further studies on monkeys with co-injection of various amount of cold raclopride to examine the relationship between the observed changes in BP_{ND} and the occupancy of receptors. Furthermore, using the present approach, it may be possible to estimate endogenous dopamine release by pharmaceutical stimuli although the interpretation of the results must be made with caution because the level of endogenous dopamine is sensitive to the timing and the response of pharmaceutical manipulation (Yoder et al., 2004).

Potential of the multiple-injection approach

The dual-injection approach is able to assess the change in BP_{ND} for receptor competition studies in a single PET scan and shortened study period, as compared to a conventional approach. However, this approach requires some caution. Firstly, the error due to residual radioactivity at the time of the second injection may affect the reliability of BP_{ND2} estimates. Therefore, we estimated the residual radioactivity, not from the measured TAC, but from a fitted TAC from the first injection. In the simulation study, with noise-added TACs, the bias and COV of BP_{ND2} estimated from the second injection were acceptable (Fig. 5).

Secondly, the administered molar amount of second injection must be same as that of the first injection for the evaluation of dopamine release, because the value of BP_{ND} decreases according to the increase in administered raclopride even if the dopamine pulse does not be released (Fig. 2B). In addition, in the dual-injection study, the radioligand for the first injection remains in the tissue at the time of second injection. Therefore, the molar amount of administered raclopride needs to be sufficiently small, that is to say, the specific activity of administered [^{11}C]raclopride should be high enough. The mass of first injection is required to be less than about 1 nmol/kg so that the remained raclopride at the second injection does not affect BP_{ND2} estimates (data not shown). To keep the amount of administered raclopride below 1 nmol/kg with the administration of 37MBq/kg [^{11}C]raclopride, its specific activity should be greater than 37 GBq/μmol. However, in the multiple-injection study, if one can synthesize [^{11}C]raclopride with high specific activity, it is an advantage that [^{11}C] raclopride, synthesized once before the scan, can be administered for both the first and second injections.

Thirdly, the timing of the second injection affected the BP_{ND} estimates, as it was also observed in the estimations using two separate conventional scans. The timing of the second injection should be fixed within the intersubjects of the group, and the interpretation of the ΔBP_{ND} requires some caution when a time–activity curve of free [^{11}C]raclopride differs. The competition paradigm also should be applied carefully in case where the dopamine released slowly in response to stimuli, because it is often difficult to estimate the timing of the dopamine peak. Despite this, we have shown that the multiple-injection approach can be used to determine a reduction in BP_{ND} values as effectively as using two separate scans, but within a single scan lasting 100 min.

The ESRTM approach can also provide ΔBP_{ND} values from a single-session scan by administering [^{11}C]raclopride using a bolus-plus-continuous (B/I) infusion approach (Zhou et al., 2006). Meanwhile, with the MI-SRTM approach, [^{11}C]raclopride can be administered several times by bolus injection, so there is no need to control the administered dose continuously, and it is easy to change the administered mass of raclopride significantly during the scan.

Since the MI-SRTM is a successor of SRTM, one advantage of the MI-SRTM is that the BP_{ND} parametric map can be obtained as shown in Fig. 8, which is crucial to perform statistical parametric mapping (SPM) type analysis. The results of our simulation and monkey studies suggest that the MI-SRTM can be applied to the estimation of ΔBP_{ND} for human study, though the optimal injection protocol needs to be evaluated. One application of the MI-SRTM approach for the human study is to estimate occupancy within short period. By the MI-SRTM approach, one can estimate the BP_{ND} value without antipsychotics and BP_{ND} with antipsychotics from one session of PET study. This approach is also useful in the estimation of receptor density (B_{max}) and affinity (K_d) that normally requires several scans with variable masses of raclopride injections (Farde et al., 1986; Doudet et al., 2003). Furthermore, this approach can be applied to other PET ligands if the BP_{ND} can be estimated by the SRTM approach.

In summary, we have developed a method for estimating the change in binding potential in a single PET scan using multiple injections of [^{11}C]raclopride and a simplified reference tissue model. Our simulations showed that the reduction in BP_{ND}, estimated by this approach, was related to the amount of released dopamine or to the administered mass of raclopride. We also demonstrated that the reduction in BP_{ND} varied according to the increase in administered raclopride in monkey studies. The proposed method, with multiple injections, has potential for use in quantitatively assessing the change in specific binding, in a short study period, for several neurotransmitter competition studies.

Acknowledgments

This research was supported by the Ministry of Education, Culture, Sports, Science and Technology, Grant-in-Aid for Young Scientists (B) (No.20790839), Japan, Kobe Cluster I and II, Ministry of Education, Culture, Sports, Science and Technology of Japan (MEXT; T.H.), and the MHLW (Ministry of Health, Labour and Welfare of Japan) Health Science Research Grant, H17-025 (T.H., H,I).

We are grateful to members of the Department of Investigative Radiology, National Cardiovascular Center Research Institute, for their support of the PET experiment and for helpful suggestions.

Please cite this article as: Ikoma, Y., et al., Quantitative evaluation of changes in binding potential with a simplified reference tissue model and multiple injections of [^{11}C]raclopride, NeuroImage (2009), doi:10.1016/j.neuroimage.2009.05.099

Appendix A

The multiple-injection simplified reference tissue model is based on the following differential equations of the simplified reference tissue model on the assumption that the time–activity curves of the target and reference tissues can be fitted to a single tissue compartment model with plasma input (Lammertsma and Hume, 1996)

$$\frac{dC_t}{dt} = K_1 C_p(t) - k_{2a} C_t(t) \tag{A1}$$

$$\frac{dC_r}{dt} = K_1^r C_p(t) - k_2^r C_t(t) \tag{A2}$$

$$K_1 / k_{2a} = K_1 / k_2 \cdot (1 + BP_{ND}) \tag{A3}$$

where C_p is the metabolite corrected plasma concentration, C_t and C_r are the concentration in target and reference tissue, respectively, k_{2a} (min^{-1}) is the apparent (overall) rate constant for transfer from specific compartment to plasma in the target tissue.

Eqs. (A1) and (A2) are expressed as follows by Laplace transform:

$$sC_t(s) - C_t(0) = K_1 C_p(s) - k_{2a} C_t(s) \tag{A4}$$

$$sC_r(s) - C_r(0) = K_1^r C_p(s) - k_2^r C_t(s) \tag{A5}$$

where $C_t(0)$ and $C_r(0)$ are the total concentration in target and reference tissue, respectively, at the time of injection.

From Eqs. (A4),(A5) and the assumption $K_1^r / k_2^r = K_1 / k_2$, the following expression can be derived:

$$C_t(s) = R_1 C_r(s) + \frac{1}{s + k_{2a}}(k_2 - Rk_{2a}) C_r(s) + \frac{1}{s + k_{2a}}(C_t(0) - R_1 C_r(0)). \tag{A6}$$

From Eqs. (A3) and (A6), the following expression can be derived by inverse-Laplace transform:

$$C_t(t) = R_1 C_r(t) + \left(k_2 - \frac{R_1 k_2}{1 + BP_{ND}}\right) e^{-\frac{k_2}{1 + BP_{ND}} t} \otimes C_r(t) + (C_t(0) - R_1 C_r(0)) e^{-\frac{k_2}{1 + BP_{ND}} t}. \tag{A7}$$

In the second injection, R_1, k_2, and BP_{ND} can be estimated by giving $C_t(t)$, $C_r(t)$, and $C_t(0)$ and $C_r(0)$ at the time of second injection. Meanwhile, in the first injection, $C_t(0)$ and $C_r(0)$ are 0 at the time of first injection, so $C_t(t)$ can be expressed as follows:

$$C_t(t) = R_1 C_r(t) + \left(k_2 - \frac{R_1 k_2}{1 + BP_{ND}}\right) e^{-\frac{k_2}{1 + BP_{ND}} t} \otimes C_r(t). \tag{A8}$$

References

Breier, A., Su, T.P., Saunders, R., Carson, R.E., Kolachana, B.S., de Bartolomeis, A., Weinberger, D.R., Weisenfeld, N., Malhotra, A.K., Eckelman, W.C., Pickar, D., 1997. Schizophrenia is associated with elevated amphetamine-induced synaptic dopamine concentrations: evidence from a novel positron emission tomography method. Proc. Natl. Acad. Sci. U.S.A. 94, 2569–2574.

Carson, R.E., Breier, A., de Bartolomeis, A., Saunders, R.C., Su, T.P., Schmall, B., Der, M.G., Pickar, D., Eckelman, W.C., 1997. Quantification of amphetamine-induced changes in [^{11}C]raclopride binding with continuous infusion. J. Cereb. Blood Flow Metab. 17, 437–447.

Christian, B.T., Narayanan, T., Shi, B., Morris, E.D., Mantil, J., Mukherjee, J., 2004. Measuring the in vivo binding parameters of [18F]-fallypride in monkeys using a PET multiple-injection protocol. J. Cereb. Blood Flow Metab. 24, 309–322.

Delforge, J., Pappata, S., Millet, P., Samson, Y., Bendriem, B., Jobert, A., Crouzel, C., Syrota, A., 1995. Quantification of benzodiazepine receptors in human brain using PET, [^{11}C] flumazenil, and a single-experiment protocol. J. Cereb. Blood Flow Metab. 15, 284–300.

Doudet, D.J., Jivan, S., Holden, J.E., 2003. In vivo measurement of receptor density and affinity: comparison of the routine sequential method with a nonsequential method in studies of dopamine D_2 receptors with [^{11}C]raclopride. J. Cereb. Blood Flow Metab. 23, 280–284.

Endres, C.J., Kolachana, B.S., Saunders, R.C., Su, T., Weinberger, D., Breier, A., Eckelman, W.C., Carson, R.E., 1997. Kinetic modeling of [^{11}C]raclopride: combined PET-microdialysis studies. J. Cereb. Blood Flow Metab. 17, 932–942.

Endres, C.J., Carson, R.E., 1998. Assessment of dynamic neurotransmitter changes with bolus or infusion delivery of neuroreceptor ligands. J. Cereb. Blood Flow Metab. 18, 1196–1210.

Farde, L., Ehrin, E., Eriksson, L., Greitz, T., Hall, H., Hedstrom, C.G., Litton, J.E., Sedvall, G., et al., 1985. Substituted benzamides as ligands for visualization of dopamine receptor binding in the human brain by positron emission tomography. Proc. Natl. Acad. Sci. U.S.A. 82, 3863–3867.

Farde, L., Hall, H., Ehrin, E., Sedvall, G., 1986. Quantitative analysis of D_2 dopamine receptor binding in the living human brain by PET. Science 231, 258–261.

Gallezot, J.D., Bottlaender, M.A., Delforge, J., Valette, H., Saba, W., Dollé, F., Coulon, C.M., Ottaviani, M.P., Hinnen, F., Syrota, A., Grégoire, M.C., 2008. Quantification of cerebral nicotinic acetylcholine receptors by PET using 2-[^{18}F]fluoro-A-85380 and the multiinjection approach. J. Cereb. Blood Flow Metab. 28, 172–189.

Gunn, R.N., Lammertsma, A.A., Hume, S.P., Cunningham, V.J., 1997. Parametric imaging of ligand–receptor binding in PET using a simplified reference region model. Neuroimage 6, 279–287.

Hall, H., Köhler, C., Gawell, L., Farde, L., Sedvall, G., 1988. Raclopride, a new selective ligand for the dopamine-D2 receptors. Prog. Neuropsychopharmacol. Biol. Psychiatry 12, 559–568.

Herzog, H., Tellmann, L., Hocke, C., Pietrzyk, U., Casey, M.E., Kuwert, T., 2004. NEMA NU2-2001 guided performance evaluation of four Siemens ECAT PET scanners. IEEE Trans. on. Nucl. Science 51, 2662–2669.

Ikoma, Y., Toyama, H., Suhara, T., 2004. Simultaneous quantification of two brain functions with dual tracer injection in PET dynamic study. In: Iida, H., Shah, N.J., Hayashi, T., Watabe, H. (Eds.), Quantitation in Biomedical Imaging with PET and MRI. InElsevier, pp. 74–78.

Ikoma, Y., Ito, H., Arakawa, R., Okumura, M., Seki, C., Shidahara, M., Takahashi, H., Kimura, Y., Kanno, I., Suhara, T., 2008. Error analysis for PET measurement of dopamine D_2 receptor occupancy by antipsychotics with [^{11}C]raclopride and [^{11}C] FLB457. Neuroimage 42, 1285–1294.

Kim, K.M., Watabe, H., Hayashi, T., Hayashida, K., Katafuchi, T., Enomoto, N., Ogura, T., Shidahara, M., Takikawa, S., Eberl, S., Nakazawa, M., Iida, H., 2006. Quantitative mapping of basal and vasareactive cerebral blood flow using split-dose ^{123}I-iodoamphetamine and single photon emission computed tomography. Neuroimage 33, 1126–1135.

Koepp, M.J., Gunn, R.N., Lawrence, A.D., Cunningham, V.J., Dagher, A., Jones, T., Brooks, D.J., Bench, C.J., Grasby, P.M., 1998. Evidence for striatal dopamine release during a video game. Nature 393, 266–268.

Koeppe, R.A., Raffel, D.M., Snyder, S.E., Ficaro, E.P., Kilbourn, M.R., Kuhl, D.E., 2001. Dual-[11C]tracer single-acquisition positron emission tomography studies. J. Cereb. Blood Flow Metab. 21, 1480–1492.

Köhler, C., Hall, H., Ogren, S.O., Gawell, L., 1985. Specific in vitro and in vivo binding of 3H-raclopride. A potent substituted benzamide drug with high affinity for dopamine D-2 receptors in the rat brain. Biochem. Pharmacol. 34, 2251–2259.

Lammertsma, A.A., Hume, S.P., 1996. Simplified reference tissue model for PET receptor studies. Neuroimage 4, 153–158.

Lammertsma, A.A., Bench, C.J., Hume, S.P., Osman, S., Gunn, K., Brooks, D.J., Frackowiak, R.S., 1996. Comparison of methods for analysis of clinical [^{11}C]raclopride studies. J. Cereb. Blood Flow Metab. 16, 42–52.

Laruelle, M., Iyer, R.N., al-Tikriti, M.S., Zea-Ponce, Y., Malison, R., Zoghbi, S.S., Baldwin, R.M., Kung, H.F., Charney, D.S., Hoffer, P.B., Innis, R.B., Bradberry, C.W., 1997. Microdialysis and SPECT measurements of amphetamine-induced dopamine release in nonhuman primates. Synapse 25, 1–14.

Logan, J., Fowler, J.S., Volkow, N.D., Ding, Y.S., Wang, G.J., Alexoff, D.L., 2001. A strategy for removing the bias in the graphical analysis method. J. Cereb. Blood Flow Metab. 21, 307–320.

Millet, P., Delforge, J., Mauguiere, F., Pappata, S., Cinotti, L., Frouin, V., Samson, Y., Bendriem, B., Syrota, A., 1995. Parameter and index images of benzodiazepine receptor concentration in the brain. J. Nucl. Med. 36, 1462–1471.

Mintun, M.A., Raichle, M.E., Kilbourn, M.R., Wooten, G.F., Welch, M.J., 1984. A quantitative model for the in vivo assessment of drug binding sites with positron emission tomography. Ann. Neurol. 15, 217–227.

Morris, E.D., Babich, J.W., Alpert, N.M., Bonab, A.A., Livni, E., Weise, S., Hsu, H., Christian, B.T., Madras, B.K., Fischman, A.J., 1996a. Quantification of dopamine transporter density in monkeys by dynamic PET imaging of multiple injections of ^{11}C-CFT. Synapse 24, 262–272.

Morris, E.D., Alpert, N.M., Fischman, A.J., 1996b. Comparison of two compartmental models for describing receptor ligand kinetics and receptor availability in multiple injection PET studies. J. Cereb. Blood Flow. Metab. 16, 841–853.

Muzic, R.R., Nelson, A.D., Saidel, G.M., Miraldi, F., 1996. Optimal experiment design for PET quantification of receptor concentration. IEEE Trans. Med. Imaging 15, 2–12.

Yoder, K.K., Wang, C., Morris, E.D., 2004. Change in binding potential as a quantitative index of neurotransmitter release is highly sensitive to relative timing and kinetics of the tracer and the endogenous ligand. J. Nucl. Med. 45, 903–911.

Watabe, H., Endres, C.J., Breier, A., Schmall, B., Eckelman, W.C., Carson, R.E., 2000. Measurement of dopamine release with continuous infusion of [^{11}C]raclopride: optimization and signal-to-noise considerations. J. Nucl. Med. 41, 522–530.

Watabe, H., Ohta, Y., Teramoto, N., Miyake, Y., Kurokawa, M., Yamamoto, A., Ose, Y., Hayashi, T., Iida, H., 2006. A novel reference tissue approach for multiple injections of [C-11]Raclopride. Neuroimage 31 (Suppl. 2), T73.

Zhou, Y., Chen, M.K., Endres, C.J., Ye, W., Brasic, J.R., Alexander, M., Crabb, AH, Guilarte, TR, Wong, D.F., 2006. An extended simplified reference tissue model for the quantification of dynamic PET with amphetamine challenge. Neuroimage 33, 550–563.

Please cite this article as: Ikoma, Y., et al., Quantitative evaluation of changes in binding potential with a simplified reference tissue model and multiple injections of [^{11}C]raclopride, NeuroImage (2009), doi:10.1016/j.neuroimage.2009.05.099

Ann Nucl Med
DOI 10.1007/s12149-009-0272-2

ORIGINAL ARTICLE

Evaluation of utility of asymmetric index for count-based oxygen extraction fraction on dual-tracer autoradiographic method for chronic unilateral brain infarction

Katsuhiro Iwanishi · Hiroshi Watabe · Hiroshi Fujisaki · Takuya Hayashi · Yoshinori Miyake · Kotaro Minato · Masaki Naganuma · Toshiyuki Uehara · Chiaki Yokota · Hiroshi Moriwaki · Katsufumi Kajimoto · Kazuhito Fukushima · Kazuo Minematsu · Hidehiro Iida

Received: 1 April 2009 / Accepted: 28 April 2009

Abstract
Objective For diagnosing patients with ischemic cerebrovascular disease, non-invasive count-based method with $^{15}O_2$ and $H_2^{15}O$ positron-emission tomography (PET) data is widely used to measure asymmetric increases in oxygen extraction fraction (OEF). For shortening study time, we have proposed dual-tracer autoradiographic (DARG) protocol in which $^{15}O_2$ gas and $C^{15}O_2$ gas are sequentially administrated within short period. In this paper, we evaluated feasibility of the non-invasive count-based method with the DARG protocol.
Methods Twenty-three patients [67.8 ± 9.9 (mean ± SD) years] with chronic unilateral brain infarction were examined by the use of measurements of asymmetric OEF elevation. As DARG protocol, $^{15}O_2$ and $C^{15}O_2$ gases were inhaled with 5-min interval and dynamic PET data were acquired for 8 min. Quantitative OEF (qOEF) image was computed with PET data and arterial input function. Ratio image of $^{15}O_2$ and $C^{15}O_2$ phases of PET data was computed as count-based OEF (cbOEF) image. The asymmetric indices (AI) of qOEF (qOEF-AI) and cbOEF (cbOEF-AI) were obtained from regions of interest symmetric placed on left and right sides of cerebral hemisphere. To optimize the summation time of PET data for the cbOEF image, qOEF and cbOEF images with various summation times were compared.
Results Image quality of cbOEF image was better than that of qOEF image. The best correlation coefficient of 0.94 was obtained when the cbOEF image was calculated from 0 to 180 s of $^{15}O_2$ summed image and 340 to 440 s of $C^{15}O_2$ summed image.
Conclusion Using the appropriate summation time, we obtained the cbOEF image with good correlation with qOEF image, which suggests non-invasive cbOEF image can be used for evaluating the degree of misery perfusion in patients with chronic unilateral brain infarction. The count-based method with DARG protocol has a potential to dramatically reduce the examination time of ^{15}O PET study.

Keywords Dual-tracer autoradiographic method · Count-based method · Oxygen extraction fraction · Asymmetric index

K. Iwanishi (✉) · H. Watabe · T. Hayashi · H. Iida
Department of Investigative Radiology,
National Cardiovascular Center Research Institute,
5-7-1 Fujishirodai, Suita, Osaka 565-8565, Japan
e-mail: kiwanish@ri.ncvc.go.jp

K. Iwanishi · K. Minato
Informatics Science, Nara Institute of Science and Technology,
Nara, Japan

H. Fujisaki · Y. Miyake · K. Fukushima
Department of Radiology and Nuclear Medicine,
National Cardiovascular Center Hospital, Osaka, Japan

M. Naganuma · T. Uehara · C. Yokota · H. Moriwaki ·
K. Kajimoto · K. Minematsu
Department of Cerebrovascular Medicine,
National Cardiovascular Center Hospital, Osaka, Japan

Introduction

Positron-emission tomography (PET) with oxygen 15 compounds can quantitatively generate the brain functional images of cerebral blood flow (CBF), oxygen extraction fraction (OEF), cerebral metabolic rate of oxygen ($CMRO_2$), and cerebral blood volume (CBV). These images are the important indices for diagnosing cerebrovascular diseases [1]. In particular, OEF image is used to

Published online: 16 June 2009

diagnose the diseases and an index of the prediction of stroke risk [2–7].

These functional images are usually computed by either steady-state method (SS method) [8–12] or autoradiographic method (ARG method) [13–18]. In SS method, quantitative images are estimated from data acquired while in the steady state reached during the continuous inhalation of $^{15}O_2$ and $C^{15}O_2$ gases. The study period with this method is long (approximately 2 h) due to the waiting time needed to reach equilibrium. The ARG method uses separate administrations of three traces of CO, CO_2, and O_2 gases [17]. The study period with the ARG method is shorter than that need with the SS method. However, a study with the ARG method still takes more than half an hour, because there is a waiting time for the decay of the residual radioactivity of the preceding tracer used. Lately, Kudomi et al. developed a dual-tracer autoradiographic method (DARG) method to shorten the PET study period [19]. This method used a single PET scan with the sequential administration of dual tracers of $^{15}O_2$ and $C^{15}O_2$ gases ($^{15}O_2$–$C^{15}O_2$ scan), and generated CBF, OEF, and $CMRO_2$ images simultaneously in an autoradiographic manner.

All methods described above require arterial blood sampling for generation of these functional images. The arterial blood sampling is labor intensive and has the possibility of blood infection. Alternatively, the ratio image of $^{15}O_2$ counts and $C^{15}O_2$ (or $H_2^{15}O$) counts assumes to be represented as relative OEF image (count-based OEF, cbOEF) [20], and has been used as the substitution of quantitative OEF (qOEF) image [5, 7, 21–24]. By the cbOEF image, one can non-invasively evaluate asymmetric increase in OEF value with a simple calculation [6, 21, 22, 24]. Recently, Kobayashi et al. investigated the optimal scan protocol for computing cbOEF to diagnose misery perfusion [25]. They concluded the cbOEF could appropriately diagnose misery perfusion when they used $^{15}O_2$ counts from 4 min after $^{15}O_2$ gas inhalation to 7 min and $H_2^{15}O$ counts for 3 min after injection of $H_2^{15}O$. In their study, continuous inhalation of $^{15}O_2$ gas and bolus injection of $H_2^{15}O$ was utilized for the administration of tracers.

In this study, we investigated the feasibility of cbOEF obtained by the DARG protocol that consists of sequential administrations of $^{15}O_2$ and $C^{15}O_2$ gases. We computed both cbOEF and qOEF images from actual PET data and both images were compared. Although, in general, the ratio image of $^{15}O_2$ counts and $C^{15}O_2$ counts is known to be proportional to qOEF image, the ratio image on the DARG protocol is special due to contamination of residual radioactivity of $^{15}O_2$ gas after inhalation of $C^{15}O_2$ gas. Therefore, we investigated the optimized range of summation time for $^{15}O_2$ counts and $C^{15}O_2$ counts in order to obtain the ratio image proportional to qOEF image. Using the DARG protocol, further shortening of examination time expects to be archived.

Materials and methods

Subjects

Subjects were 23 patients [15 men and 8 women; age (mean ± SD) 67.8 ± 9.9 years] with chronic unilateral brain infarction, which increased OEF on the unilateral side of the brain, and decreased CBF on the ipsilateral side of the brain. Selection of the data was made by visual inspection. Written informed consent was obtained from each subject prior to the study.

PET procedure

Figure 1 shows a schematic diagram of the clinical study protocol with the DARG method for our institute. The PET scanner we used was ECAT EXACT47 (CTI Inc., Knoxville, TN, USA). First, a 10-min transmission scan was performed to correct gamma ray attenuation. Then, $C^{15}O$ gas of 2500 MBq was inhaled for 30 s, and 90 s post-inhalation, a 4-min emission scan ($C^{15}O$ scan) was performed to obtain a CBV image as well as to correct vascular space in the DARG method. Finally, a single dynamic PET scan was performed with the sequential inhalation of $^{15}O_2$ gas (4000 MBq) and $C^{15}O_2$ gas (5,000 MBq) in 5-min time interval. Their inhalation period was 1 min. All radioactive gases were provided through a face mask.

For qOEF calculation, it is necessary to measure the arterial radioactivity curve as an arterial input function (AIF). A catheter was inserted into the brachial artery of the patient. As AIF, the radioactivity in the arterial blood during a $^{15}O_2$–$C^{15}O_2$ scan was continuously monitored by a GSO detector [26], with a flow rate of 3.5 ml/min. The inner diameter of the tube was approximately 2 mm, and the distance from the catheter to the detector was 20–25 cm. The arterial blood was sampled at the beginning

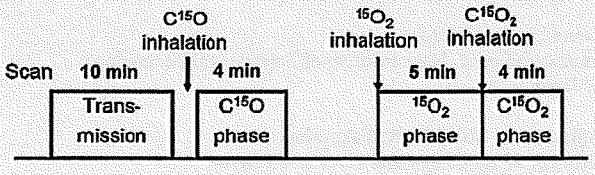

Fig. 1 The schematic diagram of clinical protocol and time schedule of DARG-PET study. The PET scan times for $C^{15}O$ and $^{15}O_2$–$C^{15}O_2$ were 4 and 8 min. The start time of $C^{15}O$ PET scan was the inhalation start time after 30 s, and the $^{15}O_2$–$C^{15}O_2$ scan start time was same the start time of inhaling $^{15}O_2$ gas

of the $C^{15}O$ scan for 30 s and the radioactivity concentration in the arterial blood was measured by a Well counter system (Shimadzu Corporation, Kyoto, Japan). The radioactivity in the sample measured by the Well counter was utilized for computing CBV image and cross-calibration between the Well counter and the GSO detector.

Quantitative OEF image

Quantitative OEF image was calculated using PET counts during $^{15}O_2$ phase $\left(\int_O C_i(t)dt\right)$ and during $C^{15}O_2$ phase $\left(\int_W C_i(t)dt\right)$, and AIF by the DARG method. The detail of the DARG method is found elsewhere [19, 27]. In brief, at first, the AIF was separated into $^{15}O_2$ ($A_{O_2}(t)$) component and $H_2^{15}O$ ($A_{H_2O}(t)$) component (note that although we used $C^{15}O_2$ gas, we used $H_2^{15}O$ for the expression in this section due to the rapid exchange of $H_2^{15}O$ by carbonate dehydratase in the lung). Then, CBF (f) was estimated using a look-up table procedure using the following equation:

$$\begin{aligned}\int_W Ci(t)dt = & f\int_W A_{H_2O}(t)\otimes \exp^{-\frac{f}{p}t}dt + V_B \\ & \cdot R_{Hct}\int_W A_{O_2}(t)dt \\ & + \left(f\int_W A_{O_2}(t)\otimes \exp^{-\frac{f}{p}t}dt + V_B\cdot R_{Hct}\cdot F_v\int_W A_{O_2}(t)dt\right) \\ & \times \frac{\int_O Ci(t) - f\int_O A_{H_2O}\otimes \exp^{-\frac{f}{p}t}dt - V_B\cdot R_{Hct}\int_O A_{O_2}dt}{f\int_O A_{O_2}\otimes \exp^{-\frac{f}{p}t}dt - V_B\cdot R_{Hct}\cdot F_v\int_O A_{O_2}dt}\end{aligned} \quad (1)$$

In the equation above, p is the blood/tissue partition coefficient of water (assumed to be 0.8 ml/ml), R_{Hct} is the small-to-large vessel hematocrit ratio (assumed to be 0.85), and V_B is the CBV obtained from $C^{15}O$ scan, and F_v is the effective venous fraction (fixed to 0.835). Finally, OEF (E) was calculated voxel-by-voxel using the equation below:

$$E = \frac{\int_O Ci(t) - f\int_O A_{H_2O}\otimes \exp^{-\frac{f}{p}t}dt - V_B\cdot R_{Hct}\int_O A_{O_2}dt}{f\int_O A_{O_2}\otimes \exp^{-\frac{f}{p}t}dt - V_B\cdot R_{Hct}\cdot F_v\int_O A_{O_2}dt} \quad (2)$$

In our DARG protocol, summation times of $^{15}O_2$ phase and $C^{15}O_2$ phase were 0–240 and 340–440 s, respectively.

Count-based OEF image

The ratio image defined as cbOEF image was defined as voxel-by-voxel ratio image of PET counts during $^{15}O_2$ phase and $C^{15}O_2$ phase. To investigate the optimal summation time for computing cbOEF against qOEF, we varied the summation time as 0–60, 0–120, 0–180, 0–240, 60–120, 60–180, 60–240, 120–180, 120–240, 180–240 s for $^{15}O_2$ phase, and 340–390, 390–440, 340–440 s for $C^{15}O_2$ phase. Therefore, the number of cbOEF images was total 30 for each subject.

Comparison of qOEF and cbOEF

In order to compare between cbOEF and qOEF, we calculate asymmetric index (AI) defined as $OEF_{vascular\ lesion\ site}/OEF_{normal\ site}$. As shown in Fig. 2, elliptic regions of interest (ROIs) (10 × 30 pixels) were drawn on 14 slices of vascular lesion site and normal site. The ROIs on the lesion site and the normal site were symmetric and there are total 28 ROIs. The all ROIs were drown on the qOEF image and superimposed to cbOEF image for each subject. The mean values within the ROIs were computed for the vascular lesion site and normal site, and the AI values for qOEF (qOEF-AI) and cbOEF (cbOEF-AI) with different summation times (total 30 patterns) were obtained. The slope of regression lines and coefficients of correlation between cbOEF-AI and qOEF-AI were calculated.

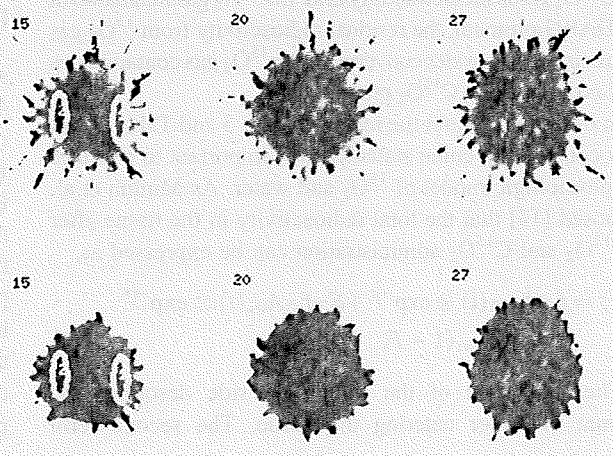

Fig. 2 This figure shows quantitative OEF images (*top*) and count-based OEF image ($^{15}O_2$ summation times 60–180 s, $C^{15}O_2$ summation time 340–440 s) (*down*) obtained on DARG method. The color scale of these images is relatively matched by normalizing maximum value of each OEF image. Ellipses in the qOEF and cbOEF images are ROIs. The size of ROIs was 10 × 30 pixels

Results

As shown in Fig. 2, cbOEF image from DARG protocol has similar image contrast against qOEF image, and better image quality (less noisy and no image artifact outside of the brain) than qOEF image. Comparisons between cbOEF-AI and qOEF-AI were carried out (Fig. 3), and correlation coefficient and slope of the regression line were summarized in Table 1. All plots except cbOEF-AI from 0 to 60 s of $^{15}O_2$ summed image have significant correlation ($P < 0.01$) against qOEF-AI. The best correlation coefficient was obtained as 0.94 when cbOEF was calculated from 0 to 180 s of $^{15}O_2$ summed image and 340–440 s of $C^{15}O_2$ summed image. However, the slope of the regression line in this case was 0.80, and cbOEF underestimated AI compared with qOEF. The slope of the regression almost became unity when cbOEF was calculated from 60 to 180 s of $^{15}O_2$ summed image and 340–390 s of $C^{15}O_2$ summed image.

Discussion

In this study, we investigated the relationship between cbOEF-AI and qOEF-AI obtained from the DARG protocol. The regression analysis was performed in order to optimize the summation time for $^{15}O_2$ phase and $C^{15}O_2$ phase in cbOEF calculation. By selecting the proper summation time, the cbOEF-AI could be utilized for diagnosing unilateral misery perfusion without arterial blood sampling.

The cbOEF image has been widely used with ^{15}O PET studies due to the simple calculation. Owing to this simplicity, the image quality of cbOEF is better than that of qOEF as shown in Fig. 2. However, since the cbOEF is empirical, in order to use the cbOEF as diagnostic tool, one must take into account of several factors such as radioactivity from blood vessel and recirculation water converted from $^{15}O_2$. The DARG protocol has another factor to be considered. Since the $C^{15}O_2$ gas is inhaled shortly after the $^{15}O_2$ gas inhalation in the DARG protocol, the residual radioactivity from $^{15}O_2$ gas and recirculation water converted from $^{15}O_2$ gas contaminates PET counts during $C^{15}O_2$ phase.

In order to interpret the results of Fig. 3 and Table 1, not only considering count statistics, it is important to consider the physiologic model of $^{15}O_2$ and water. As Mintun et al. proposed [13] that the total radioactivity in the tissue after the $^{15}O_2$ and $C^{15}O_2$ administration can be expressed as,

$$Ci(t) = f \cdot A_{H_2O}(t) \otimes \exp^{-\frac{f}{P}t} + E \cdot f \cdot A_{O_2}(t) \otimes \exp^{-\frac{f}{P}t} + V_B \cdot R_{Hct}(1 - F_v \cdot E) A_{O_2}(t) \quad (3)$$

The first term of the right-hand side describes the amount of water entering the tissue. The second term represents the amount of oxygen that enters the tissue and is immediately metabolized to water. The third term is the radioactivity of the $^{15}O_2$ in the blood vessels. After the inhalation of $^{15}O_2$ gas, the $^{15}O_2$ was metabolized in whole body as time advances, and the radioactivity of recirculation water gradually increases as the first term of the right-hand side of the Eq. 3. In general, the more the radioactivity from the recirculation water contains in the O_2 phase, the worse the cbOEF-AI correlates against qOEF-AI. As shown in Fig. 3 and Table 1, $^{15}O_2$ summation time extended to 240 s resulted in worse correlation than summation time to 180 s due to the influence of the recirculation water. If one compares between the results of the $C^{15}O_2$ summation time of 340–390 s (A) and 390–440 s (B), the slopes of (B) were smaller than (A) although the correlation coefficients for (B) were better than (A) in most cases. The count statistics of (B) was better than (A), which lead better correlation between cbOEF-AI and qOEF-AI. On the other hand, the $C^{15}O_2$ image of (B) has less contrast than (C) due to the diffusability of water, which causes the underestimation of cbOEF-AI against qOEF-AI. Because the $^{15}O_2$ image with the summation time of 0–60 s has the poorest count statistics, the cbOEF-AI with $^{15}O_2$ the summation time of 0–60 s had the worst correlation against qOEF-AI. Note that the blood component (the third term of Eq. 3) has the large influence on the $^{15}O_2$ image with summation time of 0–60 s, and the magnitude of this influence depends on the OEF value, which leads the underestimation of cbOEF-AI against qOEF-AI. Meanwhile, as judged by the best correlation coefficient, we recommend to use the following combinations:

- $^{15}O_2$ summation time of 0–180 s and $C^{15}O_2$ summation time of 340–440 s
- $^{15}O_2$ summation time of 60–180 s and $C^{15}O_2$ summation time of 340–390 s

In the latter case, the correlation coefficient was lower than one in the former, but this combination makes it possible to shorten the PET acquisition time.

Kobayashi et al. [25] reported the cbOEF-AI can be successfully used to diagnose misery perfusion if one uses 4–7 min of the summation time for continuous inhalation of $^{15}O_2$ gas in addition to 3 min of $H_2^{15}O$ PET acquisition. In their study, the waiting time between $^{15}O_2$ scan and $H_2^{15}O$ scan is necessary to avoid contamination of $^{15}O_2$ radioactivity in $H_2^{15}O$ data. Hence, the total study time for their study should be longer than 10 min. As shown in this paper, the qOEF-AI equivalent cbOEF-AI will be able to be obtained by 7.3 min after the start of $^{15}O_2$ inhalation. By using cbOEF-AI with the DARG protocol, total study time can be dramatically shortened, which is beneficial for patients as well as medical staff, and the cbOEF-AI with

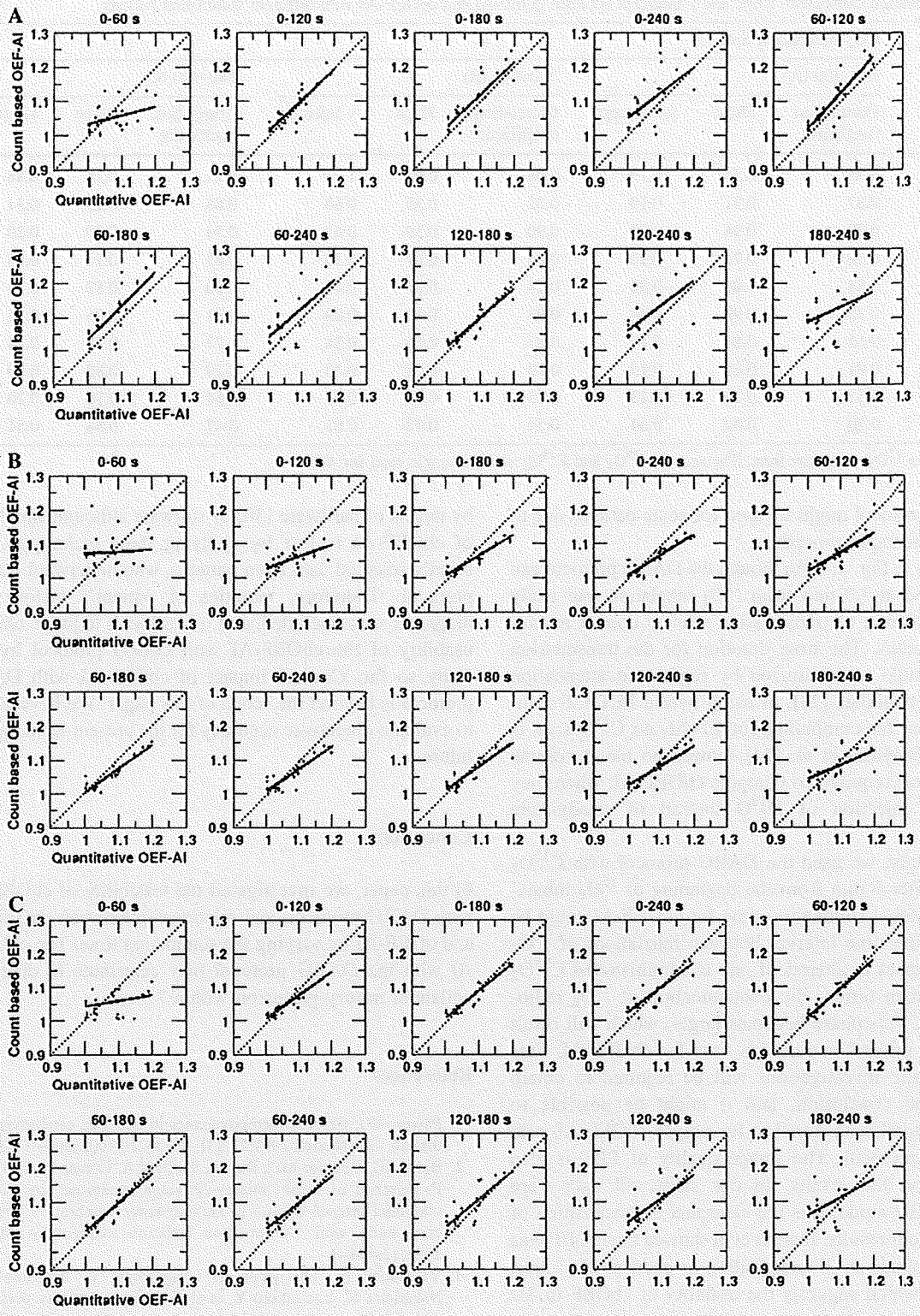

Fig. 3 These graphs show the correlation between qOEF-AI and cbOEF-AI. Each graph has different summation time for $^{15}O_2$ and $C^{15}O_2$ phases in the DARG protocol. The title of each graph represents the summation time for $^{15}O_2$ phase. The summation times for $C^{15}O_2$ phase are from 340 to 390 s for (a), 390–440 s for (b), and 340–440 s for (c)